Published in final edited form as:

Cell Metab. 2023 August 08; 35(8): 1406–1423.e8. doi:10.1016/j.cmet.2023.06.013.

Hexokinase 2-mediated gene expression via histone lactylation is required for hepatic stellate cell activation and liver fibrosis

Hyunsoo Rho[1], **Alexander R. Terry**[1,3], **Constantinos Chronis**[1], **Nissim Hay**[1,2,4,*]

[1]Department of Biochemistry and Molecular Genetics, College of Medicine, University of Illinois at Chicago, Chicago, IL 60607, USA

[2]Research and Development Section, Jesse Brown VA Medical Center, Chicago, IL 60612, USA

[3]Present address: Renaissance School of Medicine at Stony Brook University, Stony Brook, NY 11794, USA

[4]Lead contact

SUMMARY

Lactate was implicated in the activation of hepatic stellate cells (HSCs). However, the mechanism by which lactate exerts its effect remains elusive. Using RNA-seq and CUT&Tag chromatin profiling, we found that induction of hexokinase 2 (HK2) expression in activated HSCs is required for induced gene expression by histone lactylation but not histone acetylation. Inhibiting histone lactylation by *Hk2* deletion or pharmacological inhibition of lactate production diminishes HSC activation, whereas exogenous lactate but not acetate supplementation rescues the activation phenotype. Thus, lactate produced by activated HSCs determines the HSC fate via histone lactylation. We found that histone acetylation competes with histone lactylation, which could explain why class I HDAC (histone deacetylase) inhibitors impede HSC activation. Finally, HSC-specific or systemic deletion of *HK2* inhibits HSC activation and liver fibrosis *in vivo*. Therefore, we provide evidence that HK2 may be an effective therapeutic target for liver fibrosis.

Graphical abstract

*Correspondence: nhay@uic.edu.

AUTHOR CONTRIBUTIONS

Conceptualization, H.R., A.R.T., and N.H.; methodology, H.R. and C.C.; resources, H.R. and A.R.T.; investigation and visualization, H.R.; writing, H.R. and N.H.; funding acquisition and supervision, N.H.

SUPPLEMENTAL INFORMATION

Supplemental information can be found online at https://doi.org/10.1016/j.cmet.2023.06.013.

DECLARATION OF INTERESTS

The authors declare no competing interests.

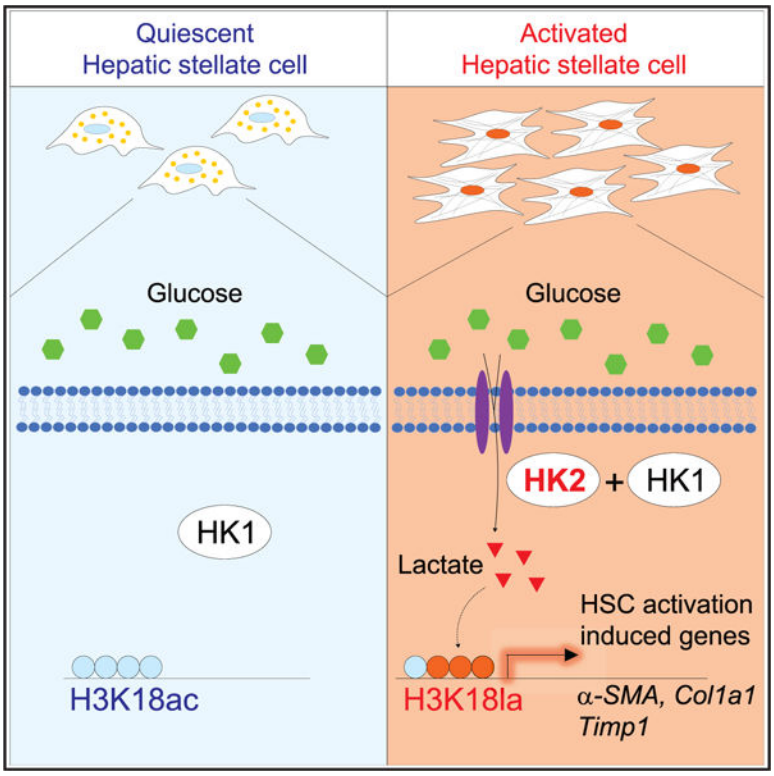

In brief

Rho et al. report that HK2-induced lactate promotes histone lactylation, which governs HSC activation and results in liver fibrosis. They demonstrate that the inhibition of H3K18la by HSC-specific or systemic deletion of HK2 mitigates HSC activation and liver fibrosis.

INTRODUCTION

Hexokinase (HK) catalyzes the first committed step in glucose metabolism by phosphorylating glucose to produce glucose-6-phosphate. This reaction captures glucose inside cells and allows cells to increase glucose utilization.[1] Among the five known HK isozymes encoded by separate genes in mammalian cells, HK1, HK2, HK3, and HKDC1 evolved from ancestral HK by evolutionary duplication and fusion of the gene.[2] However, only HK2 has two active catalytic domains in the amino and carboxyl termini of the protein, whereas HK1 and HK3 possess a single active catalytic domain in the carboxyl terminus.[1,3,4] Numerous studies have firmly established that highly glycolytic proliferating cells such as cancer cells take advantage of HK2 expression to accelerate glucose metabolism even in the presence of oxygen.[5–7] However, this acceleration not only provides sufficient glycolytic intermediates to support the anabolic demands of the cells but also inevitably accompanies increased formation of metabolic end products such as lactate.[8,9] Currently, the effect of lactate caused by HK2-mediated metabolic alteration is largely unknown.

Lactate is traditionally considered a waste product of glucose metabolism that is discarded by cells via excretion.[10] However, emerging evidence shows that lactate plays important roles as a signaling molecule, an energy substrate, and an immunoregulatory molecule.[11–13] A recent study found that lactate also plays a role in an epigenetic alteration known as histone lactylation.[14] Intriguingly, this histone modification at the lysine residues of histone tails directly promotes gene transcription similar to histone acetylation, the most widely studied histone modification, but the gene expression signatures regulated by histone lactylation are distinct from those regulated by histone acetylation.[14,15] Thus, exploring the potential roles of histone lactylation in various physiological and pathological processes may uncover novel therapeutic strategies for the treatment of human diseases.

Liver fibrosis is the wound healing response of the liver against various insults and is associated with severe morbidity and mortality.[16] Currently, there is no effective method to cure liver fibrosis except liver transplantation.[17] During liver injury, quiescent hepatic stellate cells (HSCs) undergo activation and transdifferentiation into alpha-smooth muscle actin (α-SMA)-positive myofibroblasts, which are the dominant contributors to collagen-producing cells in fibrotic livers.[18,19] Recently, metabolic reprogramming including aerobic glycolysis has emerged as a key feature in the activation of HSCs, and evidence suggests that inhibiting aerobic glycolysis prevents HSC activation.[20–22] Despite the observations that enhancement of aerobic glycolysis during HSC activation increases lactate production, the underlying mechanism by which lactate is related to HSC activation remains elusive.

In this study, we obtained evidence that HK2-induced lactate influences gene expression via histone lactylation and not histone acetylation. We next found that the induction of HK2 expression during HSC activation and the subsequent production of lactate promote histone lactylation at the promoters of genes that are induced during activation. Our results demonstrate that diminishing histone lactylation in HSCs through genetic deletion of *Hk2* or pharmacological inhibition of lactate production inhibits HSC activation, which is rescued by exogenous lactate supplementation. Moreover, we provide evidence that histone lactylation competes with histone acetylation, which otherwise inhibits HSC activation. Notably, we uncovered the genome-wide distribution of H3K18la and H3K18ac via CUT&-Tag in mouse primary HSCs, the numbers of which make whole-genome-level studies with conventional chromatin immunoprecipitation (ChIP) sequencing impracticable. Finally, we revealed that HSC-specific *Hk2* deletion or systemic deletion of *Hk2* in mice mitigates HSC activation and liver fibrosis.

RESULTS

The catalytic activity of HK2 induces histone lactylation but not histone acetylation

To explore whether HK2 expression and its catalytic activity influence histone lactylation, we utilized MI5–4 Chinese hamster ovary (CHO) cells that do not have detectable HK gene expression and have limited HK activity.[23] We expressed either wild-type (WT) HK2 or kinase-dead mutant (SA) HK2 in these cells. In the mutant, alanine was substituted for serine residues in the amino- and carboxy-terminal domains required for catalytic activity (S155A/S603A).[6,24] As shown in Figure 1A, both WT and SA HK2 were expressed at the same levels in MI5–4 CHO cells. However, extracellular acidification rate (ECAR)

measurement with a Seahorse metabolic bioanalyzer revealed significant increases in glycolytic activity only in WT HK2 cells (Figures 1B and 1C). The glycolytic activity of WT HK2 cells also resulted in significant induction of lactate production and cellular lactate levels (Figures 1D and S1A).

To determine whether lactate production induced by HK2 is sufficient to promote histone lactylation in cells, we examined lactylation on histone H3 lysine 18 (H3K18la). This lysine residue is also acetylated (H3K18ac). Interestingly, H3K18la was barely detectable in empty vector (EV) and SA HK2 cells but was highly elevated in WT HK2 cells, while H3K18ac was detectable regardless of HK2 expression, with a slight reduction in WT HK2 cells (Figure 1E). In addition to H3K18la, we found that H3K9la, H3K14la, H4K8la, and H4K12la were also elevated only in WT HK2 cells (Figure S1B). We also observed that lactylation of non-histone proteins was mostly elevated in WT HK2 cells, while most acetylation of non-histone proteins was not increased but even lowered in WT HK2 cells despite more cellular acetyl-CoA levels (Figures S1C–S1E). To further elucidate the potential functional significance of H3K18la and H3K18ac, we next performed CUT&Tag, a novel genome-wide immunotethering assay.[25] Analysis of the genome-wide distribution of H3K18la and H3K18ac showed that both histone modifications were located mainly within the promoter regions (≤3 kb) (Figures 1F and S1F). In line with our immunoblot assay results, we also observed that H3K18la peaks were increased near transcription start sites (TSSs) in WT HK2, but H3K18ac peaks were not; H3K18ac peaks were even slightly decreased (Figure 1G).

In an effort to identify potential candidate genes regulated by H3K18la and H3K18ac, we first compared these histone modification levels at the promoter regions of the same genes by following the criteria described previously for macrophages.[14] Most genes were marked by increased H3K18la without any significant induction of H3K18ac in WT HK2 cells (Figures 1H and 1I). None of the genes were marked by increased H3K18ac only in WT HK2 cells. Thus, although HK2 expression, by increasing glycolysis, can increase both lactate and acetyl-CoA levels, it exclusively affects histone lactylation. Next, we identified common H3K18la-marked candidate genes after the expression of WT HK2 compared with EV and SA HK2 and found a total of 3,003 genes (Figure S1G).

H3K18la-marked genes are involved in the regulation of gene expression and various metabolic processes

To investigate how HK2 expression and lactate affect global gene expression via histone lactylation, we first optimized histone lactylation levels through exogenous lactate treatment. We found that 10 mM lactate treatment for 24 h in EV cells induced H3K18la levels comparable to those in WT HK2 cells (Figures 2A, S2A, and S2B). We next performed RNA sequencing (RNA-seq) to compare the transcriptomes of control cells (EV), WT HK2 cells, and control cells treated with lactate (EV + Lac). Our differentially expressed gene (DEG) analysis revealed that exogenous lactate treatment changed gene expression with a pattern similar to that observed in WT HK2 cells by commonly upregulating 1,109 genes (68.5% in WT HK2 and 62.7% in EV + Lac) and downregulating 1,532 genes (75.6% in WT HK2 and 75.0% in EV + Lac) (Figures 2B, 2C, and S2C). Next, we identified

493 genes that were upregulated by both HK2 and lactate treatment, which were also marked with H3K18la at their promoter regions (Figure 2D; Table S1). In our analysis of gene ontology (GO) biological process (GOBP) terms, H3K18la-marked genes were involved in the regulation of gene expression, RNA and protein metabolic processes, and protein modification processes (Figure 2E; Table S2). The expression of selected genes with enriched GOBP terms, including canopy FGF signaling regulator 2 (*Cnpy2*), the transcription elongation factor *Supt4a*, serine- and arginine-rich splicing factor 11 (*Srsf11*), mitochondrial transcription rescue factor 1 (*Mtres1*), tissue inhibitor of metalloproteinases 1 (*Timp1*), and small proline-rich protein 1a (*Sprr1a*), was confirmed by qPCR in EV, WT HK2, SA HK2, and EV + Lac cells (Figure 2F). In addition, H3K18la and H3K18ac peaks were validated at the promoters of the selected genes, and marked increases in H3K18la peaks and slight decreases in H3K18ac peaks were observed in WT HK2 cells (Figure 2G).

To further demonstrate the relationship between HK2 expression and histone lactylation, we generated MI5–4 cells expressing inducible HK2. Induced glycolytic activity due to induced HK2 expression was confirmed according to elevations in the ECAR and oxygen consumption rate (OCR) (Figures S2D–S2G). In line with our findings regarding the constitutive expression of HK2, we observed that the induction of inducible HK2 expression also induced H3K18la with concomitant induction of gene expression, whereas reducing HK2 expression to basal levels abrogated this effect (Figures S2H and S2I). Collectively, these results demonstrate that HK2 expression elevates glycolytic activity and lactate production, which influences gene expression through H3K18la.

H3K18la is induced in activated mouse and human HSCs

Recent studies have shown that enhanced glycolysis is not only restricted to cancer cells but also occurs in fibroblasts and myofibroblasts in the liver, lungs, and kidneys during chronic inflammation and fibrosis.[17,26–29] Upon liver injury, quiescent HSCs are activated and become the major population of myofibroblasts in the fibrotic liver.[18] Although numerous studies have shown that HSC activation accompanies lactate production via induction of various glycolytic enzymes, how lactate is linked to HSC activation is still unknown.[20,22] Based on our findings above in MI5–4 CHO cells, we hypothesized that HK2-producing lactate may affect gene expression via histone lactylation during HSC activation. To test this hypothesis, we first confirmed HK2 expression in murine models of liver fibrosis caused by CCl_4 injection or bile duct ligation (BDL). We observed that HK2 expression was mostly colocalized with α-SMA-expressing myofibroblasts in the fibrotic liver (Figures S3A and S3D). We subsequently assessed the mRNA level of *Hk2* with additional HSC activation-induced genes, including collagen type 1α1 (*Col1a1*) and *Timp1*, and observed positive correlations between *Hk2* and HSC activation-induced gene expression levels in the fibrotic liver (Figures S3B, S3C, S3E, and S3F). We next isolated primary HSCs from mouse livers. The purity of the HSC population was examined by evaluating the autofluorescence of retinoid droplets (Figure S3G). Our immunoblot analysis showed that HK2 expression was robustly induced in primary HSCs from the livers of CCl_4-injected mice, whereas HK1, which is already expressed in quiescent HSCs from healthy livers, was only slightly induced in activated HSCs (Figure 3A). Quiescent HSCs can be spontaneously activated in *in vitro* culture. Consistently, HK2 expression was undetectable in quiescent HSCs, but strong

induction of HK2 expression was observed along with α-SMA expression in mouse primary HSCs cultured for 3 and 7 days (Figure 3B). Robust induction of HK2 but not HK1 was also validated at the mRNA level in primary HSCs from CCl_4-injected mouse liver (Figure S3H) as well as HSCs from BDL mouse liver (publicly accessible RNA-seq dataset GEO: GSE154170) and from 7-day *in vitro* culture (publicly accessible microarray dataset GEO: GSE34949) (Figures S3I and S3J). However, the major HK isoform in the liver, glucokinase (GCK), was expressed in mouse primary hepatocytes but not in quiescent and activated HSCs (Figure S3K). Next, measurement of the ECAR, lactate production, and cellular lactate levels showed a strong elevation of glycolytic activity in activated HSCs (Figures 3C and S3L–S3N), resulting in H3K18la induction during both *in vivo* and *in vitro* activation (Figures 3D and 3E). Importantly, in addition to H3K18la, H3K9la, H3K14la, H4K8la, and H4K12la were induced in *in vitro*-activated HSCs (Figure S3O). Unlike H3K18la, H3K18ac was present in quiescent HSCs, and its levels were sustained in *in vivo*-activated HSCs but repressed during *in vitro* activation, suggesting that HSC activation may require H3K18la but not H3K18ac. In line with histone lactylation and acetylation, we also found that non-histone lactylation was primarily elevated in *in vitro*-activated HSCs, but acetylation was mainly reduced (Figures S3P and S3Q). To reinforce our findings in the clinical context in humans, we performed double immunofluorescence staining of human liver tissues from patients with cirrhosis. Immunostaining of patient livers indicated that 82.9% ± 3.1% of α-SMA^+ cells expressed HK2, 63.0% ± 5.2% of the cells expressed H3K18la, and 78.2% ± 3.6% of $COL1α1^+$ cells expressed HK2, and H3K18la was expressed in 66.6% ± 5.1% (Figure 3F), supporting the link of HSC activation with HK2 expression and H3K18la presence. Overall, these results suggest that induced HK2 expression and glycolytic activity may play a role in mouse and human activated HSCs via H3K18la.

H3K18la is enriched at the promoter regions of genes that are induced in activated HSCs

To further determine whether H3K18la plays a role in gene expression during HSC activation, we performed genome-wide CUT&Tag in mouse primary HSCs freshly isolated from healthy livers or cultured for 6 days. Intriguingly, H3K18la in activated HSCs was distributed mostly within the promoter regions (42.5%), whereas H3K18ac was distributed to a much lesser extent (27.4%) at the promoter regions, even less than in introns (28.2%) and distal intergenic regions (34.5%) (Figures 3G and S3R). These findings suggest that H3K18la, but not H3K18ac, plays a major role in the induction of gene expression during HSC activation. By analyzing the promoter region, we identified 4,070 genes as H3K18la-marked candidate genes, 117 genes that share H3K18la and H3K18ac, and only 20 genes as H3K18ac-marked candidate genes (Figure 3H). Thus, the vast majority of genes in activated HSCs are marked by H3K18la at the promoter region. To identify H3K18la-marked genes in activated HSCs, RNA-seq was conducted in primary HSCs cultured for 6 days, and this revealed 1,677 genes that were significantly upregulated and 1,505 genes that were significantly downregulated during activation (Figure 3I). Finally, we identified 1,126 genes that were upregulated with the induction of H3K18la at the promoter region (Figure 3J; Table S3). GOBP term analysis revealed that these H3K18la-marked genes were involved in cell adhesion, migration, and wound healing (Figure 3K; Table S4), suggesting that H3K18la may regulate key genes representing major HSC characteristics.

Genetic deletion of *Hk2* inhibits HSC activation by reducing H3K18la, which is rescued by exogenous lactate but not acetate supplementation

Given our findings that activated HSCs undergo metabolic reprogramming by inducing glycolysis along with HK2 expression and H3K18la, we speculated that HK2 ablation impedes HSC activation by inhibiting H3K18la. To test our hypothesis, primary HSCs were isolated from the liver of $Hk2^{f/f}$ mice, and genetic deletion was conducted via exposure to an adenovirus expressing Cre recombinase fused to eGFP (Ad-GFP-Cre) followed by culture for 6 days (Figure S4A). *Hk2* deletion in HSCs reduced the ECAR, lactate production, and cellular lactate levels by approximately 60% (Figures 4A–4C and S4B). The OCR was also diminished significantly (Figures S4C and S4D), indicating that HK2 expression promotes the induction of the major portion of glycolysis upon HSC activation to provide pyruvate, which is both reduced to lactate and oxidized in mitochondria, where cellular respiration occurs. Furthermore, this metabolic perturbation caused by *Hk2* deletion inhibited α-SMA expression and proliferation but did not cause cell death (Figures 4D, S4E, and S4F). As expected, the activation of WT primary HSCs was unaffected by adenoviral Cre transduction (Figure 4D).

Having identified the effects of *Hk2* ablation on glycolytic activity and HSC activation, we next examined the levels of H3K18la and H3K18ac. Interestingly, *Hk2*-deleted cells displayed lower levels of H3K18la and H3K18ac than activated HSCs, but exogenous lactate treatment recovered H3K18la, whereas H3K18ac was further decreased (Figure 4E). Consistently, heatmap analysis of the CUT&Tag results showed marked induction of H3K18la near the TSSs of genes in activated mouse primary HSCs, which was diminished by *Hk2* deletion and was recovered after the addition of lactate (Figure 4F). In contrast, H3K18ac was reduced in activated HSCs and was further reduced by *Hk2* deletion and lactate treatment (Figure 4F). To further investigate whether H3K18la-marked genes are dependent on HK2 expression as well as lactate treatment, we compared the expression of H3K18la-marked genes in activated WT HSCs with activated HK2-knockout (KO) HSCs. We found an approximately 3-fold increase in downregulated genes in activated HK2-KO cells (Figure 4G). Lactate treatment reversed the expression of most genes that were dependent on HK2 expression (Figure 4H; Table S5). GOBP term analysis showed that these bona fide genes dependent on HK2/H3K18la and lactate treatment were related to cell adhesion, migration, extracellular matrix organization, and TGF-β receptor signaling pathways (Figure S4G; Table S6), implying a key role of HK2/H3K18la in the regulation of HSC activation-induced genes. Indeed, H3K18la peaks were highly enriched at the promoters of key induced genes in activated HSCs but not in quiescent and HK2-KO cells, but lactate treatment in HK2-KO cells restored H3K18la peaks (Figures 4I, 4J, and S4H–S4J). Consistent with our findings regarding genome-wide H3K18ac peaks near TSSs, H3K18ac peaks were gradually suppressed at the promoters of the genes in activated HK2-KO cells as well as in HK2-KO cells treated with lactate.

Supplementation with acetate is known to augment histone acetylation and chromatin accessibility.[30] To assess whether lactate and acetate treatments recover gene expression in HK2-KO HSCs, we measured the transcript levels of HSC activation-induced genes. Surprisingly, lactate treatment upregulated gene expression that was repressed by *Hk2*

deletion, but acetate treatment did not (Figure 4K). Likewise, the invasive ability of activated HSCs was diminished by *Hk2* deficiency but rescued by lactate treatment, while the phenotype was not restored by acetate treatment (Figure 4L). Collectively, our findings show that *Hk2* deletion inhibits HSC activation, which is rescued by lactate treatment (likely through H3K18la) but not by acetate treatment.

Pharmacological inhibition of lactate production inhibits HSC activation, which is rescued by exogenous lactate but not acetate

In a continuing effort to investigate the relationship between histone lactylation and HSC activation, we further assessed the activation of gene expression upon treatment with pharmacological inhibitors of lactate production. Oxamate and dichloroacetate (DCA) have been evaluated as anticancer drugs because of their ability to modulate glycolysis.[31,32] Oxamate inhibits lactate production from pyruvate by inhibiting lactate dehydrogenase (LDH), whereas DCA inhibits lactate production by increasing the conversion of pyruvate to acetyl-CoA instead of to lactate by inhibiting pyruvate dehydrogenase kinase (PDHK) (Figure 5A). As previously reported, oxamate and DCA treatments significantly reduced lactate production and cellular lactate levels (Figures 5B, 5C, and S5A), and this intervention inhibited cell proliferation without causing cell death in mouse primary HSCs (Figures 5D and S5B). Oxamate and DCA treatments effectively decreased H3K18la along with the expression of HSC activation-induced genes, which were rescued by lactate but not by acetate supplementation (Figures 5E–5H). In an effort to further define the direct relationship between LDH and HK2-induced histone lactylation and subsequent gene expression, small interfering RNA (siRNA) targeting *Ldha* was transfected in mouse primary HSCs. Consistent with LDH inhibitor treatment, siRNA knockdown of *Ldha* attenuated cellular lactate levels and H3K18la together with HSC activation-induced gene expression, which were restored by lactate but not by acetate treatment (Figures S5C–S5E).

TGF-β1 is considered a key cytokine that plays essential roles in fibrogenic signaling pathways in HSCs.[33] Recently, increasing evidence has demonstrated that TGF-β1 also participates in metabolic reprogramming by enhancing glycolytic flux in HSCs and fibroblasts.[22,27] Although Lx-2 human HSCs are considered constitutively activated, TGF-β1 further activates these cells. We therefore examined the effect of TGF-β1 on Lx-2 cell activation. As expected, TGF-β1 increased lactate production, an effect that was diminished by oxamate or DCA treatment (Figure S5F). Reducing the glucose level from 25 to 5 mM decreased H3K18la, but TGF-β1 increased H3K18la while decreasing H3K18ac at both glucose concentrations (Figure S5G). As expected, both *α-SMA* gene expression and *COL1A1* gene expression were induced by TGF-β1 (Figure S5H). Our subsequent time course studies revealed that H3K18la was continuously increased at later time points (6–24 h) after TGF-β1 treatment, which was correlated with the significant upregulation of HSC-activation-induced genes (Figures S5I and S5J). In contrast, the H3K18ac level was slightly increased at 1 h, but this increase was followed by a continuous reduction after TGF-β1 treatment (Figure S5I). To ascertain the effect of TGF-β1 on the histone modification of the α-SMA gene promoter in Lx-2 cells, we performed ChIP-qPCR to analyze histone lactylation and acetylation at the promoter region. Consistent with our immunoblot results, TGF-β1 increased H3K18la but decreased H3K18ac on the α-SMA

promoter (Figure S5K). Next, we found that oxamate and DCA reduced H3K18la and inhibited the α-SMA expression elevated by TGF-β1 (Figures S5L, S5N, S5Q, and S5S). We further confirmed that this inhibition was not due to cell death (Figures S5M and S5R). In our rescue experiments, reduced expression of activation-induced genes was recovered by lactate but not by acetate treatment (Figures S5O, S5P, S5T, and S5U). Our findings suggest that interfering with lactate production reduces H3K18la and the expression of HSC activation-induced genes, which can be recovered by lactate but not by acetate supplementation. Taken together, these results show that histone lactylation plays a critical role in HSC activation and the subsequent induction of gene expression.

Class I HDAC inhibitors elevate H3K18ac but repress H3K18la and thus inhibit the expression of HSC activation-induced genes

Histone deacetylases (HDACs) catalyze the removal of acetyl groups from histone lysine residues, resulting in chromatin condensation that suppresses gene transcription.[34] Previous studies have shown that inhibition of class I HDACs, which are exclusively localized in the nucleus, inactivates HSCs *in vitro* and *in vivo*.[35–37] Considering our findings that H3K18la is a novel histone modification that mirrors the expression of HSC-activation-induced genes, we postulated that class I HDAC inhibitors may induce H3K18ac, which competes with H3K18la on the same lysine 18 residue on histone H3. First, we treated activated mouse primary HSCs with the class I HDAC inhibitors apicidin and MS275 (entinostat) (Figure 5I). Inhibitor treatment increased H3K18ac but decreased H3K18la, suggesting the existence of competition between acetylation and lactylation on lysine 18 (Figure 5J). Next, apicidin and MS275 treatment significantly lowered the activation of gene expression and proliferation, and these effects were not due to cell death (Figures 5K, S5V, and S5W). To further explore the possibility of competition between histone lactylation and acetylation, we treated Lx-2 cells with lactate and acetate. Lactate treatment alone increased α-SMA expression, but acetate treatment alone showed the opposite effect (Figures S5X and S5Y). Interestingly, the lactate-induced expression of α-SMA was abolished when acetate was also added (Figure S5Z). Indeed, H3K18la was highly elevated by lactate treatment, but this elevation was inhibited when acetate was also added and thus H3K18ac levels recovered (Figure S5AA). Hence, our findings suggest that class I HDAC inhibitors may inactivate HSCs by upregulating H3K18ac, which competes with H3K18la, resulting in the downregulation of H3K18la-dependent gene expression.

HSC-specific and systemic deletion of *Hk2* inhibits liver fibrosis *in vivo*

To further corroborate the role of HK2/H3K18la in HSCs in the context of liver fibrosis, we first generated $Hk2^{f/f};Lrat^{Cre}$ mice in which *Hk2* could be specifically deleted in HSCs.[18] The mice were injected with CCl_4 for 3 weeks to induce liver fibrosis (Figure 6A). Sirius red and Masson's trichrome staining showed that the accumulation of collagen caused by CCl_4 was markedly decreased in the liver when *Hk2* was deleted in HSCs (Figures 6B and 6E). In parallel with collagen deposition, α-SMA expression was significantly reduced in HSC-specific HK2-KO mouse livers (Figures 6B and 6D). To validate whether the H3K18la level reflects the HSC activation *in vivo*, we isolated mouse primary HSCs from the livers of $Hk2^{f/f}$ or HSC-specific HK2-KO mice after CCl_4 administration. We confirmed that the induced H3K18la level in mouse primary HSCs from the liver after

CCl_4 administration was markedly decreased by *Hk2* deficiency (Figure 6C). However, the H3K18ac level was not changed. Next, measurement of ALT (alanine transaminase) and AST (aspartate transaminase) showed that *Hk2* deletion in HSCs did not significantly affect hepatotoxicity (Figure 6F). Given that exogenous lactate supplementation rescued HSC activation phenotype in *Hk2*-deleted HSCs *in vitro*, we next assessed the effect of lactate in HSC-specific HK2-KO mice by injecting 2 g/kg lactate (intraperitoneally [i.p.], pH 7.4) every other day for 3 weeks during CCl_4 injection (Figure S6A). Interestingly, our Sirius red and α-SMA immunostaining results showed that decreased collagen deposition and α-SMA expression in HSC-specific HK2-KO mouse liver were restored by the addition of lactate *in vivo* (Figures S6B and S6C). Together, our findings suggest that HSC-specific deletion of *Hk2* mitigates H3K18la in HSCs and inhibits liver fibrosis, whereas chronic and systemic lactate treatment *in vivo* restores collagen deposition and α-SMA expression.

We have previously shown that systemic *Hk2* deletion in adult mice is well tolerated and therapeutic for breast and lung cancer without adverse physiological consequences.[6] To provide proof of concept that HK2 is a therapeutic target for liver fibrosis, we emulated drug therapy by employing $Hk2^{f/f};UBC^{CreERT2}$ mice, which harbor ubiquitously expressed tamoxifen-inducible Cre recombinase. $Hk2^{f/f};UBC^{CreERT2}$ mice were treated with tamoxifen when they were 6–7 weeks old, as previously described,[6] and effective HK2 ablation was confirmed in adult tissues in which HK2 was expressed (Figures S7A and S7B). In our single-dose CCl_4-challenge experiment, we observed that hepatocytes in zone 3 (centrilobular) were similarly damaged in both *Hk2*-proficient and systemically *Hk2*-deficient mice (Figures S7C and S7F). However, α-SMA expression was significantly inhibited in the livers of mice with systemic *Hk2* deletion (Figures S7C–S7E). We next challenged mice with systemic *Hk2* deletion with CCl_4 treatment for 3 weeks (Figure 7A). Notably, our Sirius red and Masson's trichrome staining results demonstrated that collagen accumulation was markedly repressed in the liver after *Hk2* systemic deletion (Figures 7B and 7D). In addition, a significant reduction in the α-SMA expression was confirmed (Figures 7B and 7C). To further analyze the antifibrotic effect of systemic *Hk2* deletion, we next established a BDL-induced fibrosis model in $Hk2^{f/f};UBC^{CreERT2}$ mice after tamoxifen injection (Figure 7F). In line with our findings in previous *in vivo* experiments, systemic *Hk2* deletion effectively inhibited collagen accumulation and α-SMA expression in the livers of BDL-subjected mice (Figures 7G–7I). In CCl_4-induced and BDL-induced fibrosis models, serum ALT and AST activities were similar between the *Hk2*-proficient and *Hk2*-deficient groups, suggesting that systemic *Hk2* deletion *in vivo* does not cause remarkable cytotoxicity (Figures 7E and 7J). Next, to further understand the effect of systemic *Hk2* deletion in the therapeutic potential, we first induced liver fibrosis by CCl_4 treatment for 3 weeks and then attempted to delete *Hk2* systemically (Figure 7K). In systemic *Hk2*-deleted mouse liver, Sirius red and Masson's trichrome staining showed significantly reduced collagen deposition (Figures 7L and 7M). We observed that α-SMA expression was also diminished when *Hk2* was systemically deleted after liver fibrosis was established (Figure 7N). Moreover, serum ALT and AST activities were not significantly affected when *Hk2* was deleted after the induction of liver fibrosis (Figure 7O). Last, in the experiment of control $UBC^{CreERT2}$ mice treated with CCl_4 for 3 weeks, the Sirius red-positive area and α-SMA expression were not affected by tamoxifen (Figures S7G–S7J), which suggested

that the decrease in HSC activation after systemic *Hk2* deletion was not a side effect of Cre activity. Taken together, our results show that targeting HK2 systemically inhibits HSC activation; thus, HK2 may be a therapeutic target for liver fibrosis.

DISCUSSION

Induction of glucose metabolism by HK2 may affect, in addition to glycolysis, the pentose phosphate pathway and the hexosamine pathway.[1,38] Recently, it has been shown that HK2 exhibits noncatalytic activity as an A-kinase anchoring protein.[24] In this study, we obtained evidence that lactate produced as a consequence of HK2 expression can modulate gene expression via histone lactylation. In HK-null MI5–4 cells, catalytically active HK2 enhanced H3K18la at the promoters of genes, but a kinase-dead mutant did not. Recent studies have suggested that aerobic glycolysis is a feature of HSC activation, and inhibiting aerobic glycolysis effectively reduces HSC activation *in vitro*.[20,22,39,40] Moreover, pharmacological inhibition of glycolytic enzymes attenuates liver fibrosis *in vivo*.[21,40] Previous studies have also implied that lactate, which is produced by HSCs immediately after their activation, participates in subsequent steps of HSC activation, including gene expression.[20,22] However, the mechanism by which lactate exerts its effect has remained elusive. Here, we show that the lactate production mediated by the induction of HK2 expression in HSCs is critical for the induction of gene expression via histone lactylation. We demonstrate that HK2-mediated H3K18la plays a critical role in the activation of HSCs, whose persistent activation culminates in liver fibrosis. Our data show that H3K18la, a previously unappreciated histone modification in HSCs, is enriched at the promoters of genes that are induced following HSC activation. Interfering with lactate production via *Hk2* deletion, LDH inhibition, or PDHK inhibition reduces H3K18la and results in HSC inactivation. In addition to H3K18la, we observed that histone lactylation on different lysine residues of H3 and H4 histones is also elevated in activated HSCs. A recent study has proposed that H4K12la is elevated at the promoters of glycolytic genes such as *Pkm* and *Ldha* to form a positive feedback loop in glycolysis and gene expression in microglia in an Alzheimer's disease mouse model.[41] It will be interesting to further explore the potential roles of H4K12la and other histone lactylation modifications in HSC activation and liver fibrosis.

Another important finding of our study is that HK2 affects only H3K18la induction, not H3K18ac, at the promoter regions of HSC-activation-induced genes. Furthermore, our findings show that while H3K18la is increased, H3K18ac is reduced during HSC activation, and there is competition between H3K18 lactylation and acetylation. Previously, it was shown that HDAC inhibition in HSCs, which elevates histone acetylation, inhibits HSC activation.[35–37] We here confirm that class I HDAC inhibitors inhibit the expression of HSC activation-induced genes. Mechanistically, our results suggest that inhibitor treatment induces H3K18ac and thus interferes with H3K18la by competing for the same histone lysine residue. Recently, class I HDAC was also suggested as a histone delactylase.[42] In the study, significant histone delactylase activity was demonstrated in peptide-based *in vitro* assays, while H3K18la modification was unaffected in Hela cells when class I HDACs were overexpressed or knocked down. Thus, these and our findings imply that the complexity of histone modification dynamics exists in cells. Nonetheless, we carefully surmise that class I

HDAC inhibition reduces H3K18la and represses HSC activation-induced gene expression at least in HSCs.

Recently, histone and DNA methylation has been reported as a drug-targetable epigenetic modification in HSC activation and liver fibrosis.[43,44] The small molecule CM272 is a dual inhibitor of histone lysine methyltransferase G9a and DNA methyltransferases (DNMTs).[45] Interestingly, CM272 treatment decreases DNA methylation and histone methylation, which inactivate HSCs by mitigating the glycolytic phenotype and lactate production.[44] Although the antifibrotic effect of CM272 is attributed to its effect on histone and DNA methylation, we speculate that the reduction in lactate production caused by CM272 treatment may also reduce histone lactylation and therefore HSC activation. Together with our results, these results imply that histone lactylation and methylation, but not histone acetylation, orchestrate an important epigenetic modification required for HSC activation.

Studying epigenetic modification in primary HSCs is crucial because primary HSCs can be used to obtain more accurate information on quiescent phenotypes and activated phenotypes. The use of primary cells also bypasses the artifacts and limitations inherent to the use of immortalized cell lines.[46] However, achieving genome-wide epigenetic studies with primary HSCs is challenging because of the limited number of cells, as conventional ChIP sequencing typically requires a few million cells, which are impracticable to collect. CUT&Tag is a newly invented immunotethering assay that innovatively reduces the requirement to fewer than a few thousand cells.[25,47] CUT&Tag also improves the signal-to-noise ratio by an order of magnitude, substantially reducing the amount of sequencing required to map chromatin features. In our study, we applied this new methodology to display H3K18la and H3K18ac in quiescent, activated, *Hk2*-deleted, and *Hk2*-deleted, lactate-treated mouse primary HSCs. Considering that a comprehensive overview of epigenetic modifications is important for understanding HSC activation, our study may provide insights to aid future epigenomics studies on primary HSCs.

In summary, we have revealed that HK2-mediated lactate production affects gene expression via histone lactylation. We show that the induction of HK2 expression in activated HSCs is crucial for HSC activation and that histone lactylation resulting from HK2 expression determines gene expression following HSC activation. Furthermore, our results show that intervention in the HK2/H3K18la axis is a potential therapeutic strategy for liver fibrosis.

Limitations of the study

Although our study unveils that the promoter of HSC activation-induced genes is marked by H3K18la during HSC activation, we also found that enhanced glycolysis during activation affected different lysine residues on H3 and H4 as well as non-histone proteins by lactylation. Future studies to define the functional involvement of lysine lactylation on various histone and non-histone proteins during HSC activation are necessary to better comprehend the associated impact on liver fibrosis. Another limitation is that cellular lactyl-CoA, the activated form of lactate to modify lysine residue, was not measured due to the technical limitation to accurately quantify lactyl-CoA in mammalian cells. Although cellular glycolytic activity and lactate levels positively correlate with histone lactylation

levels, improved quantitative methodologies may uncover previously unknown mechanisms by which histone lactylation is regulated.

STAR★METHODS

RESOURCE AVAILABILITY

Lead contact—Further information and requests for resources and reagents should be directed to and will be fulfilled by the lead contact, Nissim Hay, nhay@uic.edu.

Materials availability—This study did not generate new unique reagents.

Data and code availability

- The RNA-seq and CUT&Tag datasets reported in this study have been deposited in the NCBI Gene Expression Omnibus (GEO) under accession number GSE229151, GSE229153, GSE229154, GSE229155 in the Super Series GSE229156. Original data for creating all graphs in the paper are provided in Data S1.
- This paper does not report original code.
- Any additional information required to reanalyze the data reported in this paper is available from the lead contact upon request.

EXPERIMENTAL MODEL AND SUBJECT DETAILS

Human study—Human liver tissue sections from patients with cirrhosis were purchased from TissueArray.com (https://tissuearray.com/, MD). Both male and female individuals were included. 5 μm thick consecutive sections were investigated for α-SMA and HK2 or H3K18la, or COL1A1 and HK2 or H3K18la double immunofluorescence staining. Tissue information is provided in the key resources table.

***In vivo* animal studies—**All mice in this study were from the C57BL/6 background. $Lrat^{Cre}$ mice were kindly provided by Dr. Robert F. Schwabe (Columbia University, NY). To generate $Hk2^{f/f};Lrat^{Cre}$ mice, $Hk2^{f/f}$ mice were crossed with $Lrat^{Cre}$ mice. $Hk2^{f/f};UBC^{CreERT2}$ mice were generated by crossing the $Hk2^{f/f}$ and $UBC^{CreERT2}$ strains as previously described.[6] The mice were housed at 20 ± 2 °C with 12 h light/dark cycles and a relative humidity of 50 ± 5% under filtered, pathogen-free air, with food and water available *ad libitum*. To induce mouse liver fibrosis, six- to seven-week-old WT male mice were *i.p.* injected with vehicle (corn oil) or 0.5 ml/kg CCl_4 twice a week for five weeks. The mice were sacrificed two days after the final CCl_4 injection. For BDL-induced fibrosis, six- to seven-week-old WT male mice were subjected to a sham operation or BDL surgery as previously described.[59] Briefly, the abdomen of mice was opened followed by common bile duct separation from portal vein and hepatic artery. Next, 5–0 suture was placed around the common bile duct and secure it with two surgical knots. After second ligation was performed in the same manner, abdominal layers were closed. After the surgery, mice were subjected to 1 mg/kg buprenorphine solution (SR-LAB) subcutaneously. The mice were sacrificed two weeks after BDL surgery. To examine the effect of systemic *Hk2* deletion

on liver fibrosis, six- to seven-week-old *Hk2*$^{f/f}$;*UBC*^{CreERT2} mice were *i.p.* injected with 1 mg tamoxifen (T5648, Sigma−Aldrich) for five consecutive days to recombine the *Hk2* allele using the *UBC*^{CreERT2} system. After three weeks, mouse tail samples were used for genotyping to confirm systemic *Hk2* allele recombination. Then, systemic *Hk2*-deleted mice were *i.p.* injected with 0.5 ml/kg CCl_4 twice a week for three weeks (CCl_4-induced fibrosis) or subjected to BDL surgery and sacrificed after two weeks (BDL-induced fibrosis). For a control experiment, *UBC*^{CreERT2} mice were treated with 1 mg tamoxifen for five consecutive days and then injected with CCl_4 (0.5 ml/kg i.p.) twice a week for three weeks. To examine the effect of systemic *Hk2* deletion in established liver fibrosis, six- to seven-week-old *Hk2*$^{f/f}$ or *Hk2*$^{f/f}$;*UBC*^{CreERT2} mice were *i.p.* injected with 0.5 ml/kg CCl_4 twice a week for three weeks. From the last day of CCl_4 injection, mice were *i.p.* injected with 1 mg tamoxifen for five consecutive days to systemically delete Hk2. The mice were sacrificed seven days after the final CCl_4 injection. To examine the effect of lactate in HSC specific *Hk2* deleted mice, *Hk2*$^{f/f}$ or *Hk2*$^{f/f}$;*Lrat*^{Cre} mice were injected with vehicle (corn oil) or CCl_4 (0.5 ml/kg i.p.) twice a week for three weeks. During CCl_4 injection, mice were *i.p.* injected with sodium lactate (2 g/kg in PBS, pH 7.4) every other day for three weeks. The mice were sacrificed two days after the final CCl_4 injection. All animal experiments were approved by the University of Illinois at Chicago Institutional Animal Care and Use Committee.

METHOD DETAILS

Primary HSC isolation—Primary HSCs were isolated from adult C57BL/6 mice as previously described with minor modifications.[60] Briefly, four to five mice were subjected to retrograde liver perfusion *in situ* with pronase (P5147, Sigma−Aldrich), collagenase (LS004194, Worthington), and deoxyribonuclease (LS002139, Worthington). Next, the livers were dissected, and the cell suspension was pooled, filtered with a cell strainer (70 μm) and transferred into 50 mL falcon tubes. Nonparenchymal cells were collected from the supernatant after centrifugation at 30 × g for 5 min. Next, nonparenchymal cells were centrifuged at 700 × g for 10 min and washed with Gey's balanced salt solution (GBSS)/B buffer twice before being subjected to density gradient centrifugation with Nycodenz (AN1002424, Accurate Chemical and Scientific Corporation) at 1,380 × g for 17 min without braking. The purity of HSCs was evaluated by retinoid autofluorescence under a Zeiss LSM 700 confocal microscope.

Cell culture—MI5–4 CHO cells were kindly provided by Dr. John Wilson (Michigan State University, MI). The pLenti-6-D-TOPO-Blast lentiviral vector (Invitrogen) was used for overexpression of the following HA-tagged HKs: rat WT HK2 and a rat catalytic HK2 mutant (SA: S155A/S603A). Transduced MI5–4 cells were antibiotic-selected with blasticidin for 7–10 days. The cells were then removed from the antibiotic selection medium and cultured in Minimum Essential Medium alpha (MEM-α; M3852–02, US Biological Life Sciences) containing 1,000 mg/L glucose supplemented with 10% fetal bovine serum and 1% penicillin−streptomycin at 37 °C in a humidified atmosphere with 5% CO_2. For the doxycycline-inducible HK2 overexpression system, HA-tagged rat WT HK2 was inserted into the pCW-puro lentiviral vector. Transduced MI5–4 cells were antibiotic-selected with puromycin for 7–10 days. The cells were then removed from the antibiotic selection medium

and cultured in MEM-α medium containing 1,000 mg/L glucose supplemented with 10% tetracycline-negative fetal bovine serum and 1% penicillin−streptomycin at 37 °C in a humidified atmosphere with 5% CO_2. For transient induction of HK2 expression, cells were treated with 1 μg/ml doxycycline for 3 days. To switch off HK2 expression, doxycycline was withdrawn for 10 days after transient induction. The Lx-2 cell line was kindly supplied by Dr. Scott L. Friedman (Icahn School of Medicine at Mount Sinai, NY). To obtain activated mouse primary HSCs, cells were maintained for 7 days in Dulbecco's modified Eagle's medium (DMEM) containing 1,000 mg/L glucose supplemented with 10% fetal bovine serum and 1% penicillin− streptomycin at 37 °C in a humidified atmosphere with 5% CO_2. To generate *Hk2*-deleted HSCs, primary HSCs were isolated from adult $Hk2^{f/f}$ mice. Then, the cells were exposed to adenoviruses expressing either eGFP (VVC-U of Iowa-4, UI Viral Vector Core) or Cre recombinase fused to eGFP (VVC-U of Iowa-1174, UI Viral Vector Core) at a multiplicity of infection (MOI) of 1,000. After 48 h of incubation, the medium was replaced, and the cells were collected after 6 days. The effects of lactate (L7022, Sigma−Aldrich) were evaluated in CHO cells as indicated in the figure legends. The effects of lactate and acetate (S5636, Sigma−Aldrich) were evaluated in mouse primary HSCs and Lx-2 cells. For oxamate (A16532, Alfa Aesar) or DCA (347794, Sigma−Aldrich) treatment, mouse primary HSCs were treated on day 1 and day 3. Cells were treated with lactate or acetate on day 3 and collected on day 5. Lx-2 cells were pretreated for 6 h with oxamate or for 3 h with DCA followed by TGFβ1 with either lactate or acetate. All drugs were pH-neutralized before treatment. For class I HDAC inhibitor treatment, mouse primary HSCs were treated with apicidin (A8176, ApexBio) or MS275 (A8171, ApexBio) on day 5, and cells were collected on day 7.

Immunoblotting—Cells were centrifuged at 3,000 × g for 5 min, and lysates were prepared using RIPA buffer on ice for 1 h. The lysates were centrifuged at 13,000 × g for 10 min to obtain supernatants. The proteins in the lysates were resolved by SDS-polyacrylamide gel electrophoresis and were transferred to nitrocellulose membranes. The immobilized proteins were immunoblotted with antibodies against the proteins of interest. The bands were visualized using an enhanced chemiluminescence (ECL) system (GE Healthcare, UK) or a LI-COR Odyssey imaging system (Lincoln, Nebraska). Equal loading of proteins was verified by immunoblotting for β-actin. All the antibodies used in immunoblot analysis are listed in the key resources table.

Histone extraction—Histones were extracted using a standard acid-extraction protocol.[61] Briefly, cell pellets were incubated in hypotonic lysis buffer (10 mM Tris-HCl pH 8.0, 1 mM KCl, 1.5 mM $MgCl_2$, 1 mM DTT) for 30 min at 4 °C with rotation. The intact nuclei were resuspended in 0.4 N H_2SO_4 for approximately 4 h at 4 °C with rotation. The cleared histone extracts were precipitated by adding 1 volume of 100% TCA to 2 volumes of sample (final concentration of TCA: 33%) for 1 h on ice. Afterward, the histone pellet was washed twice with ice-cold acetone and air-dried. The samples were quantified by measuring the absorbance at 230 nm, and equal amounts of histone were loaded onto a 15% SDS−PAGE gel. Equal loading of histones was verified by immunoblotting for total histone H3.

RNA isolation and qRT−PCR assays—Total RNA was extracted using TRIzol (15596–018, Invitrogen) and reverse-transcribed into complementary DNA (cDNA) with an iScript cDNA Synthesis Kit (1708890, Bio-Rad). qRT−PCR was carried out using a CFX96 real-time PCR instrument (Bio-Rad) and iQ SYBR Green Supermix (1708880, Bio-Rad) according to the manufacturers' instructions. A melting curve was created for each amplicon to verify its accuracy. The levels of target mRNAs were normalized to those of β-actin. The primer sequences are listed in Table S7.

Histopathology and immunohistochemistry—Mouse liver specimens were fixed in 10% formalin, embedded in paraffin, cut into 5 μm thick sections and mounted on slides. Paraffin-embedded tissue sections were deparaffinized with xylene and rehydrated with an alcohol series. After antigen retrieval was performed, endogenous peroxidase was quenched with 3% H_2O_2 for 10 min. Then, 5% normal goat serum (S-1000, Vector Laboratories) was applied for blocking for 30 min at room temperature, and the tissues were incubated anti-α-SMA antibody (1:200, ab7817, Abcam) overnight at 4 °C. ImmPRESS anti-rabbit or anti-mouse IgG polymer reagent (MP-7401 or MP-7402, Vector Laboratories) was applied for 30 min, and the slides were developed using a DAB substrate kit (SK-4100, Vector Laboratories) before being subjected to hematoxylin counterstaining. For Sirius red staining, a solution of Picro-Sirius red was applied for 1 h, after which 2 changes of 0.5% acetic acid solution and absolute alcohol were performed. The Sirius red-positive area was quantified from 7–8 randomly selected fields of x100 magnification per slide by NIH ImageJ software. For Masson's trichrome staining, staining was carried out according to the manufacturer's instructions (ab150686, Abcam). Briefly, deparaffinized sections were incubated with Bouin's Fluid for 1 h at 60 °C. Weigert's iron hematoxylin was applied for 5 min, after which Biebrich scarlet/Acid fuchsin solution was applied for 15 min. The slides were differentiated in phosphomolybdic/phosphotungstic acid solution for 15 min and incubated in aniline blue solution for 10 min. Finally, the slides were incubated in acetic acid solution for 5 min, dehydrated and mounted. For quantification of α-SMA IHC staining, the IHC Profiler ImageJ plugin was used as described previously.[58] This plugin enables the color deconvolution of hematoxylin (blue) and DAB (brown) pixels. The cytoplasmic stained image mode was selected, and H DAB vectors were used. The IHC Profiler macro-outputs of high positive and positive were assigned as 4 and 3 according to the scoring formula. The IHC intensity score was calculated by the following IHC optical density score equation [(Percentage contribution of high positive x 4 + Percentage contribution of positive × 3)/100].

Immunofluorescence staining—For human α-SMA and HK2 or H3K18la, or COL1A1 and HK2 or H3K18la double staining, liver tissue section slides from cirrhotic patients were purchased from TissueArray.com (https://tissuearray.com/, MD). Tissue section was deparaffinized with xylene and rehydrated with an alcohol series. After antigen retrieval was performed, endogenous peroxidase was quenched with 3% H_2O_2 for 10 min. Normal goat serum (5%, S-1000, Vector Laboratories) was applied for blocking for 30 min at room temperature, and then the tissues were incubated with an anti-α-SMA antibody (1:200, ab7817, Abcam), an anti-COL1A1 antibody (1:200, 66948, Cell Signaling Technology), an anti-HK2 antibody (1:150, 22029–1-AP, Proteintech), an anti-H3K18la antibody (1:100,

PTM-1406, PTM Biolabs) overnight at 4 °C followed by Alexa Fluor 488-conjugated goat anti-rabbit IgG (1:500, A-11008, Thermo Fisher Scientific) and Alex Fluor 594-conjugated goat anti-mouse IgG (1:500, A-11005, Thermo Fisher Scientific) for 1 h room temperature. For mouse HK2 and α-SMA double staining, liver sections were incubated with an anti-HK2 antibody (1:50, 22029–1-AP, Proteintech) and an anti-α-SMA antibody (1:200, ab7817, Abcam) followed by Alexa Fluor 488-conjugated goat anti-rabbit IgG (1:500, A-11008, Thermo Fisher Scientific) and Alexa Fluor 594-conjugated goat anti-mouse IgG (1:500, A-11005, Thermo Fisher Scientific) for 1 h room temperature. Imaging analysis was performed using a Zeiss LSM 700 confocal microscope. HK2 and H3K18la positive populations among α-SMA or COL1α1 positive cells were quantified via QuPath.[57]

Serum alanine transaminase (ALT) and aspartate transaminase (AST) measurement—Mouse whole blood was collected and left at room temperature for 30 min. The clots were removed by centrifugation at 5,000 rpm for 15 min. Serum ALT activity was determined with an EnzyChrom ALT Assay Kit (EALT-100, BioAssay Systems) and serum AST activity was determined with an EnzyChrom AST Assay Kit (EASTR-100, BioAssay Systems) according to the manufacturer's instructions.

RNA-Seq and data analysis—Total RNA was extracted from CHO cells and mouse primary HSCs using a Direct-zol RNA MicroPrep Kit (R2060, Zymo Research) according to the manufacturer's instructions. The RNA purity, concentration, and integrity were evaluated with an Agilent TapeStation 4200 (Agilent Technologies). CHO cell RNA libraries were prepared using a Nugen Universal Plus mRNA-seq library preparation kit, and the indexed libraries were subjected to sequencing on an Illumina NovaSeq 6000 (2 × 150 bp) at the Genome Research Core at the University of Illinois at Chicago (UIC). Read mapping was performed via STAR[48] using CHOK1GS from Ensembl as a reference genome. Differential expression analysis was implemented using edgeR,[49] and only genes for which the average counts per million (cpm) value was larger than 20 in each group were retained. Mouse primary HSC RNA libraries were prepared using an Illumina TruSeq Stranded mRNA Sample Prep kit, and the indexed libraries were subjected to sequencing on an Illumina NovaSeq 6000 (2 × 150 bp) at Roy J. Carver Biotechnology Center (CBC) at the University of Illinois at Urbana-Champaign (UIUC). Read mapping was performed via Kallisto[50] using UCSC mm10 as the reference genome. Differential expression analysis was implemented using edgeR, and the overlapping genes in mouse primary HSC CUT&Tag were retained. For both CHO and primary HSCs, GO analysis was carried out using the DAVID database in *mus musculus* background (https://david.ncifcrf.gov). The *P*-value represents the modified Fisher exact test-corrected Expression Analysis Systematic Explorer (EASE) score.

CUT&Tag chromatin profiling—CHO cells and mouse primary HSCs were harvested, counted, and centrifuged at 600 × g for 3 min at room temperature. A total of 100,000 cells/sample were subjected to CUT&Tag as previously described.[47] Briefly, the cells were incubated with NE1 buffer (20 mM HEPES pH 7.9, 10 mM KCl, 0.1% Triton X-100, 20% glycerol, 0.5 mM spermidine, EDTA-free protease inhibitor) on ice for 10 min. After collecting nuclear pellets, concanavalin A-coated magnetic beads (21–1401, EpiCypher) were mixed in thin-walled PCR tubes and incubated for 10 min at room temperature.

Next, the unbound supernatant was removed, and the bead-bound cells were resuspended in antibody buffer (20 mM HEPES pH 7.5, 150 mM NaCl, 0.5 mM spermidine, EDTA-free protease inhibitor, 0.01% digitonin, 2 mM EDTA). H3K18la (PTM-1406, PTM Biolabs), H3K18ac (ab1191, Abcam) and anti-IgG negative control (13–0042, EpiCypher) antibodies were added, and the samples were incubated on a nutator overnight at 4 °C. The primary antibodies were removed by placing the tubes on a magnetic stand to clear the samples and drawing off all the liquid. Then, incubation with 0.5 μg of secondary antibody was performed on a nutator for 1 h at room temperature followed by incubation with pAG-Tn5 in 300-wash buffer (20 mM HEPES pH 7.5, 300 mM NaCl, 0.5 mM spermidine, EDTA-free protease inhibitor, 0.01% digitonin) for 1 h at room temperature. After washing with 300-wash buffer two times, the bead/nucleus pellet was resuspended in tagmentation buffer (300-wash buffer including 10 mM $MgCl_2$), and the mixture was incubated for 1 h at 37 °C. Next, the bead/nucleus pellet was resuspended in TAPS buffer (10 mM TAPS pH 8.5, 0.2 mM EDTA). The bead/nucleus pellet was then resuspended in SDS release buffer (10 mM TAPS pH 8.5, 0.1% SDS) and incubated for 1 h at 58 °C. Next, SDS quenching buffer (0.67% Triton X-100) was added. To amplify the libraries, 2 μl of a universal i5 and a uniquely barcoded i7 primer (10 μM stocks)[62] were added. A volume of 25 μl of NEBNext High-Fidelity 2x PCR Master mix (M0541, New England Biolabs) was added and mixed. The samples were placed in a thermocycler with a heated lid using the following cycling conditions: 58 °C for 5 min; 72 °C for 5 min; 98 °C for 45 sec; 14 cycles of 98 °C for 15 sec and 60 °C for 10 sec; final extension at 72 °C for 1 min; and hold at 8 °C. Post-PCR clean-up was performed by adding 1.3x AMPure XP beads (A63880, Beckman Coulter), and the libraries were incubated with the beads for 10 min at room temperature, washed twice gently in 80% ethanol, and eluted in 15 μ of 10 mM Tris pH 8.0. The tubes were placed on a magnetic stand, and the liquid was withdrawn into a fresh tube. Next, the size distribution of libraries was determined with an Agilent TapeStation 4200 (Agilent Technologies), and the libraries were mixed to achieve equal representation. Paired-end (2 × 50 bp) Illumina sequencing was performed at the Single Cell Sequencing Pilot at the University of Illinois at Chicago.

CUT&Tag data analysis—For analysis of the CUT&Tag data from CHO cells, paired-end reads were mapped to CHOK1GS from Ensembl as a reference genome using Bowtie2[51] version 2.4.4 with the options –local -very-sensitive -no-mixed -no-discordant -phred33 -I 10 -X 700. Reads with an alignment quality score less than 2 were removed with the samtools[52] view -q option. We performed peak calling using SEACR[53] in '0.01 norm stringent' mode. The reads in the promoter region (+3 kb to −1 kb) of each gene were counted, and the overlapping genes in RNA-seq were retained, after which the genes with average counts greater than 20 in each group were filtered. For analysis of the CUT&Tag data from mouse primary HSCs, the paired-end reads were mapped to the mouse reference genome UCSC mm10 using Bowtie2 with the options –local -very-sensitive -no-mixed -no-discordant -phred33 -I 10 -X 700. Reads with an alignment quality score less than 2 were removed with the samtools view -q option. We performed peak calling using SEACR with '0.01 norm stringent' mode, the reads in the promoter region (+3 kb to −1 kb) of each gene were counted, and the overlapping genes in RNA-seq were retained. The genes for which the sum of the average counts was greater than 50

were filtered. To annotate the locations of peaks in genomic features, BED files were used to perform peak annotation with ChIPseeker.[54] To visualize the genomic occupancy of the peaks ± the 3 kb flanking TSSs, BAM files were converted to BIGWIG files with the bamCoverage function of deepTools[55] with the parameter '–normalizeUsing RPKM' and 'computeMatrix', 'plotHeatmap' functions were applied. For genome browser representation, the BIGWIG files were loaded using the Integrative Genomics Viewer (IGV).[56]

ChIP-qPCR assay—Lx-2 cells (9×10^6) were seeded on 15 cm plates and treated with TGFβ1 (1 ng/ml) for 24 h. The cells were crosslinked with 1% formaldehyde for 10 min, and crosslinking was quenched with 0.125 M glycine for 5 min at room temperature. Then, the cells were washed three times with ice-cold PBS and collected. The cells were lysed on ice for 10 min in lysis buffer (50 mM Tris-HCl pH 8.0, 10 mM EDTA pH 8.0, 1% SDS). Next, the lysed cells were sonicated with a Misonix sonicator 3000 (9 W; 20 sec on; 40 sec off; total length 3 min), and an average fragment size of 200~500 bp was confirmed by agarose gel electrophoresis. Anti-H3K18la (PTM-1427RM; 2 μg), anti-H3K18ac (ab1191; 2 μg), and anti-IgG (3900S; 2 μg) antibodies were used for immunoprecipitation. The precipitated DNA fragments containing the α-SMA promoter were quantitated by qPCR using the primers described in key resources table.

Measurement of the ECAR and OCR—ECAR and OCR measurements were performed using an XF96e Extracellular Flux analyzer (Agilent Technologies). CHO cells (10,000 cells per well) and mouse primary HSCs (30,000 cells per well for vehicle group; 10,000 cells per well for CCl_4 group) were directly seeded onto XF96 cell culture plates the day before the experiment to acquire 70–80% confluence. The next day, the growth medium in the wells was replaced with XF assay medium (XF base medium lacking bicarbonate and HEPES containing 25 mM glucose, 4 mM glutamine for OCR measurements, and 4 mM glutamine only for ECAR measurement), and the plate was transferred to a 37 °C CO_2-free incubator for 1 h. For ECAR measurement, glucose, oligomycin and 2-deoxyglucose were added to final concentrations of 10 mM, 2 μM and 100 mM, respectively. For OCR measurement, oligomycin, FCCP and rotenone/antimycin A were added to final concentrations of 2 μM, 2 μM and 1 μM, respectively. In a typical experiment, 3 baseline measurements were taken prior to the addition of any compound, and 3 response measurements were taken after the addition of each compound. The ECAR and OCR were normalized to the cell number as determined by a Celigo Imaging Cytometer (Nexcelom Bioscience) at the end of the experiments. Each experiment was performed at least three times in triplicate.

Measurement of metabolites—For cellular acetyl-CoA measurement, CHO cells were washed and harvested in PBS. Harvested cells were divided into two tubes, and one tube was deproteinized by perchloric acid (PCA), and the other tube was homogenized in RIPA buffer. After centrifugation, supernatant of PCA was recovered and neutralized by the addition of potassium bicarbonate until the pH of the sample was in the range of 6–8, and precipitates were removed by centrifugation. The supernatant was used to determine acetyl-CoA concentration by using an Acetyl-CoA Assay Kit (MAK039, Sigma-Aldrich) according

to manufacturer's instructions. Supernatant of RIPA buffer was used to determine protein concentration by Pierce Rapid Gold BCA protein Assay Kit (A53225, Thermo scientific) according to manufacturer's instructions. The acetyl-CoA concentration was normalized to protein concentration of each sample.

For cellular lactate measurement, CHO cells and mouse primary HSCs were washed and harvested in Lactate Assay Buffer provided by Picoprobe L-Lactate Assay Kit (ab169557, abcam), and then homogenized. After centrifugation, supernatant was recovered and used to determine L-lactate concentration by using Picoprobe L-Lactate Assay Kit and protein concentration by Pierce Rapid Gold BCA protein Assay Kit according to the manufacturer's instructions. The lactate concentration was normalized to protein concentration of each sample.

The concentration of lactate in the medium was measured with a YSI 2700 Select biochemistry analyzer (YSI, Yellow Springs, OH) according to the manufacturer's instructions. Briefly, CHO cells or Lx-2 cells were seeded at a density of 2×10^4 cells per well in 48-well plates the day before the experiment. The next day, the medium was replaced with 250 μl of fresh medium, and the medium was collected after 24 h. Lx-2 cells were incubated with TGFβ1 (1 ng/ml), oxamate (20 mM), and DCA (20 mM). Mouse primary HSCs were seeded in equal numbers per well in 48-well plates and treated with oxamate (5 mM) or DCA (5 mM) on day 1 and day 3. On day 3 of treatment, the medium was replaced with 250 μl of fresh medium, and the medium was collected after 24 h. *Hk2*-deleted or corresponding mouse primary HSCs were collected in culture after 6 days and seeded at a density of 2×10^4 cells per well in 48-well plates the day before the experiment. The next day, the medium was replaced with 250 ml of fresh medium, and the medium was collected after 24 h. The lactate concentration was determined by subtracting the value for cell-free medium from the value for cell-containing medium and normalized to the cell number as determined by a Celigo Imaging Cytometer (Nexcelom Bioscience) at the end of the experiments.

siRNA transfection—Equal numbers of mouse primary HSCs were plated on 12-well plates and then subjected to siRNA transfection on day 1 and day 4 by following the manufacturer's instructions with 1 μl of Lipofectamine 2000 (11668019, Invitrogen), using siRNA pools targeting mouse Ldha (L-043884–00-0005, Dharmacon) or non-targeting control (D-001810–01-05, Dharmacon) at 40 pmol per well. After 6 h, transfection medium was replaced by cell growth medium. On day 6, medium was freshly replaced, and cells were treated either 10 mM lactate or acetate for 24 h, prior to terminal assays.

Matrigel invasion assay—*Hk2*-deleted or corresponding mouse primary HSCs were collected in culture after 6 days, and 3×10^4 cells per well were seeded in Corning BioCoat Matrigel Invasion Chambers with 8.0 μm PET Membrane (354480, Corning Incorporated). After 12 h, the non-invading cells were removed from the upper surface of the Matrigel with a cotton swab. The invaded cells were fixed and stained with hematoxylin and eosin (H&E). The invaded cells were counted in 3–5 randomly selected fields of x100 magnification per slide.

Cell viability assay—Lx-2 cells were plated at a density of 5×10^4 cells per well in 24-well plates. The next day, the medium was replaced with 500 μl of fresh medium, and the cells were incubated with TGFβ1 (1 ng/ml), oxamate (20 mM), and DCA (20 mM) for 24 h. Equal numbers of mouse primary HSCs were plated on 24-well plates and then treated with oxamate (5 mM) or DCA (5 mM) on day 1 and day 3, and the assay was performed on day 5. For apicidin (1 μM) and MS275 (1 μM) treatment, mouse primary HSCs were cultured for 5 days and then treated for 48 h. *Hk2*-deleted mouse primary HSCs were assayed after 6 days in culture. Then, 100 μl of staining solution (8 μM Hoechst 33342; 0.4 μg/ml propidium iodide [PI]) was added, and the cells were incubated for 20 min. The stained cells were counted by a Celigo Imaging Cytometer (Nexcelom Bioscience), and PI-negative cells were considered viable cells [i.e., Viability (%) = 100 x (PI negative cells in the well)/(total cells in the well)].

BrdU cell proliferation assay—Equal numbers of mouse primary HSCs were plated on 24-well plates and then subjected to *Hk2* deletion, treatment with oxamate (5 mM) or DCA (5 mM) on day 1 and day 3, or culture for 5 days and treatment with apicidin (1 μM) or MS275 (1 μM). Then, BrdU incorporation was performed in the cells with 10 μM BrdU labeling medium for 24 h, and the cells were fixed with 100% methanol for 20 min at −20 °C. For denaturation of DNA and permeabilization of the cells, the medium was replaced with 2 M HCl/0.5% Triton X-100 for 1 h, after which 0.1 M sodium borate was added for 10 min. The cells were then washed and incubated with an anti-BrdU antibody (1:500, M0744, Dako) overnight at 4 °C. The next day, the cells were washed and incubated with Alexa Fluor 594-conjugated goat anti-mouse IgG (1:250, A-11005, Thermo Fisher Scientific) for 2 h at room temperature and then subjected to Hoechst 33342 nuclear staining. BrdU-positive cells were examined and quantified by a Celigo Imaging Cytometer (Nexcelom Bioscience).

QUANTIFICATION AND STATISTICAL ANALYSIS

Statistically significant differences were assessed by two-tailed unpaired Student's *t* test or one-way analysis of variance (ANOVA) followed by Tukey's or SNK multiple comparisons test. The data are expressed as the mean ± SEM. The criterion for statistical significance was set at $P<0.05$ or $P<0.01$.

Supplementary Material

Refer to Web version on PubMed Central for supplementary material.

ACKNOWLEDGMENTS

N.H. acknowledges support from NIH grants R01AG016927, R01CA090764, R01CA206167, and R01CA258299; the VA merit awards BX000733 and BX005092; and the VA research career scientist award IK6BX004602. H.R. acknowledges support from the Center for Clinical and Translational Science. A.R.T. acknowledges support from F30CA225058. We thank UIC Genome Research Core, Research Informatics Core, SCS Pilot, and UIUC DNA Services Core for their help with next-generation sequencing experiments. We thank Dr. Robert F. Schwabe (Columbia University, NY) for providing LratCre mice. We thank Dr. Steven Henikoff (Fred Hutchinson Cancer Center, WA) for helpful discussions on CUT&Tag experiments. We thank Dr. Yingming Zhao (University of Chicago, IL) for providing resources and helpful discussions.

REFERENCES

1. Hay N (2016). Reprogramming glucose metabolism in cancer: can it be exploited for cancer therapy? Nat. Rev. Cancer 16, 635–649. 10.1038/nrc.2016.77. [PubMed: 27634447]
2. Irwin DM, and Tan H (2008). Molecular evolution of the vertebrate hexokinase gene family: identification of a conserved fifth vertebrate hexokinase gene. Comp. Biochem. Physiol. Part D Genomics Proteomics 3, 96–107. 10.1016/j.cbd.2007.11.002. [PubMed: 20483211]
3. Ardehali H, Yano Y, Printz RL, Koch S, Whitesell RR, May JM, and Granner DK (1996). Functional organization of mammalian hexokinase II. Retention of catalytic and regulatory functions in both the NH2- and COOH-terminal halves. J. Biol. Chem 271, 1849–1852. 10.1074/jbc.271.4.1849. [PubMed: 8567628]
4. Roberts DJ, and Miyamoto S (2015). Hexokinase II integrates energy metabolism and cellular protection: akting on mitochondria and TORCing to autophagy. Cell Death Differ 22, 248–257. 10.1038/cdd.2014.173. [PubMed: 25323588]
5. DeWaal D, Nogueira V, Terry AR, Patra KC, Jeon SM, Guzman G, Au J, Long CP, Antoniewicz MR, and Hay N (2018). Hexokinase-2 depletion inhibits glycolysis and induces oxidative phosphorylation in hepatocellular carcinoma and sensitizes to metformin. Nat. Commun 9, 446. 10.1038/s41467-017-02733-4. [PubMed: 29386513]
6. Patra KC, Wang Q, Bhaskar PT, Miller L, Wang Z, Wheaton W, Chandel N, Laakso M, Muller WJ, Allen EL, et al. (2013). Hexokinase 2 is required for tumor initiation and maintenance and its systemic deletion is therapeutic in mouse models of cancer. Cancer Cell 24, 213–228. 10.1016/j.ccr.2013.06.014. [PubMed: 23911236]
7. Shangguan X, He J, Ma Z, Zhang W, Ji Y, Shen K, Yue Z, Li W, Xin Z, Zheng Q, et al. (2021). SUMOylation controls the binding of hexokinase 2 to mitochondria and protects against prostate cancer tumorigenesis. Nat. Commun 12, 1812. 10.1038/s41467-021-22163-7. [PubMed: 33753739]
8. Vander Heiden MG, Cantley LC, and Thompson CB (2009). Understanding the Warburg effect: the metabolic requirements of cell proliferation. Science 324, 1029–1033. 10.1126/science.1160809. [PubMed: 19460998]
9. Lunt SY, and Vander Heiden MG (2011). Aerobic glycolysis: meeting the metabolic requirements of cell proliferation. Annu. Rev. Cell Dev. Biol 27, 441–464. 10.1146/annurev-cellbio-092910-154237. [PubMed: 21985671]
10. Rabinowitz JD, and Enerbäck S (2020). Lactate: the ugly duckling of energy metabolism. Nat. Metab 2, 566–571. 10.1038/s42255-020-0243-4. [PubMed: 32694798]
11. Brooks GA (2018). The science and translation of lactate shuttle theory. Cell Metab 27, 757–785. 10.1016/j.cmet.2018.03.008. [PubMed: 29617642]
12. Daw CC, Ramachandran K, Enslow BT, Maity S, Bursic B, Novello MJ, Rubannelsonkumar CS, Mashal AH, Ravichandran J, Bakewell TM, et al. (2020). Lactate elicits ER-mitochondrial Mg(2+) dynamics to integrate cellular metabolism. Cell 183, 474–489.e17. 10.1016/j.cell.2020.08.049. [PubMed: 33035451]
13. Zhang W, Wang G, Xu ZG, Tu H, Hu F, Dai J, Chang Y, Chen Y, Lu Y, Zeng H, et al. (2019). Lactate is a natural suppressor of RLR signaling by targeting MAVS. Cell 178, 176–189.e15. 10.1016/j.cell.2019.05.003. [PubMed: 31155231]
14. Zhang D, Tang Z, Huang H, Zhou G, Cui C, Weng Y, Liu W, Kim S, Lee S, Perez-Neut M, et al. (2019). Metabolic regulation of gene expression by histone lactylation. Nature 574, 575–580. 10.1038/s41586-019-1678-1. [PubMed: 31645732]
15. Izzo LT, and Wellen KE (2019). Histone lactylation links metabolism and gene regulation. Nature 574, 492–493. 10.1038/d41586-019-03122-1. [PubMed: 31645737]
16. Dulai PS, Singh S, Patel J, Soni M, Prokop LJ, Younossi Z, Sebastiani G, Ekstedt M, Hagstrom H, Nasr P, et al. (2017). Increased risk of mortality by fibrosis stage in nonalcoholic fatty liver disease: systematic review and meta-analysis. Hepatology 65, 1557–1565. 10.1002/hep.29085. [PubMed: 28130788]
17. Tan Z, Sun H, Xue T, Gan C, Liu H, Xie Y, Yao Y, and Ye T (2021). Liver fibrosis: therapeutic targets and advances in drug therapy. Front. Cell Dev. Biol 9, 730176. 10.3389/fcell.2021.730176. [PubMed: 34621747]

18. Mederacke I, Hsu CC, Troeger JS, Huebener P, Mu X, Dapito DH, Pradere JP, and Schwabe RF (2013). Fate tracing reveals hepatic stellate cells as dominant contributors to liver fibrosis independent of its aetiology. Nat. Commun 4, 2823. 10.1038/ncomms3823. [PubMed: 24264436]
19. Sherman MH (2018). Stellate cells in tissue repair, inflammation, and cancer. Annu. Rev. Cell Dev. Biol 34, 333–355. 10.1146/annurev-cellbio-100617-062855. [PubMed: 30028641]
20. Chen Y, Choi SS, Michelotti GA, Chan IS, Swiderska-Syn M, Karaca GF, Xie G, Moylan CA, Garibaldi F, Premont R, et al. (2012). Hedgehog controls hepatic stellate cell fate by regulating metabolism. Gastroenterology 143, 1319–1329.e11. 10.1053/j.gastro.2012.07.115. [PubMed: 22885334]
21. Mejias M, Gallego J, Naranjo-Suarez S, Ramirez M, Pell N, Manzano A, Suñer C, Bartrons R, Mendez R, and Fernandez M (2020). CPEB4 increases expression of PFKFB3 to induce glycolysis and activate mouse and human hepatic stellate cells, promoting liver fibrosis. Gastroenterology 159, 273–288. 10.1053/j.gastro.2020.03.008. [PubMed: 32169429]
22. Trivedi P, Wang S, and Friedman SL (2021). The power of plasticity-metabolic regulation of hepatic stellate cells. Cell Metab 33, 242–257. 10.1016/j.cmet.2020.10.026. [PubMed: 33232666]
23. O'Rear JL, Scocca JR, Walker BK, Kaiden A, and Krag SS (1999). Chinese hamster ovary cells with reduced hexokinase activity maintain normal GDP-mannose levels. J. Cell. Biochem 72, 56–66. 10.1002/(sici)1097-4644(19990101)72:1<56::aid-jcb7>3.0.co;2-h. [PubMed: 10025667]
24. Blaha CS, Ramakrishnan G, Jeon SM, Nogueira V, Rho H, Kang S, Bhaskar P, Terry AR, Aissa AF, Frolov MV, et al. (2022). A non-catalytic scaffolding activity of hexokinase 2 contributes to EMT and metastasis. Nat. Commun 13, 899. 10.1038/s41467-022-28440-3. [PubMed: 35173161]
25. Kaya-Okur HS, Wu SJ, Codomo CA, Pledger ES, Bryson TD, Henikoff JG, Ahmad K, and Henikoff S (2019). CUT&Tag for efficient epigenomic profiling of small samples and single cells. Nat. Commun 10, 1930. 10.1038/s41467-019-09982-5. [PubMed: 31036827]
26. Hou W, and Syn WK (2018). Role of metabolism in hepatic stellate cell activation and fibrogenesis. Front. Cell Dev. Biol 6, 150. 10.3389/fcell.2018.00150. [PubMed: 30483502]
27. Xie N, Tan Z, Banerjee S, Cui H, Ge J, Liu RM, Bernard K, Thannickal VJ, and Liu G (2015). Glycolytic reprogramming in myofibroblast differentiation and lung fibrosis. Am. J. Respir. Crit. Care Med 192, 1462–1474. 10.1164/rccm.201504-0780OC. [PubMed: 26284610]
28. Yin XN, Wang J, Cui LF, and Fan WX (2018). Enhanced glycolysis in the process of renal fibrosis aggravated the development of chronic kidney disease. Eur. Rev. Med. Pharmacol. Sci 22, 4243–4251. 10.26355/eurrev_201807_15419. [PubMed: 30024614]
29. Zhao X, Kwan JYY, Yip K, Liu PP, and Liu FF (2020). Targeting metabolic dysregulation for fibrosis therapy. Nat. Rev. Drug Discov 19, 57–75. 10.1038/s41573-019-0040-5. [PubMed: 31548636]
30. Kinnaird A, Zhao S, Wellen KE, and Michelakis ED (2016). Metabolic control of epigenetics in cancer. Nat. Rev. Cancer 16, 694–707. 10.1038/nrc.2016.82. [PubMed: 27634449]
31. Pelicano H, Martin DS, Xu RH, and Huang P (2006). Glycolysis inhibition for anticancer treatment. Oncogene 25, 4633–4646. 10.1038/sj.onc.1209597. [PubMed: 16892078]
32. Tataranni T, and Piccoli C (2019). Dichloroacetate (DCA) and cancer: an overview towards clinical applications. Oxid. Med. Cell. Longev 2019, 8201079. 10.1155/2019/8201079. [PubMed: 31827705]
33. Dewidar B, Meyer C, Dooley S, and Meindl-Beinker AN (2019). TGF-beta in hepatic stellate cell activation and liver fibrogenesis-updated 2019. Cells 8. 10.3390/cells8111419.
34. Li Y, and Seto E (2016). HDACs and HDAC inhibitors in cancer development and therapy. Cold Spring Harb. Perspect. Med 6. 10.1101/cshperspect.a026831.
35. Claveria-Cabello A, Colyn L, Arechederra M, Urman JM, Berasain C, Avila MA, and Fernandez-Barrena MG (2020). Epigenetics in liver fibrosis: could HDACs be a therapeutic target? Cells 9. 10.3390/cells9102321.
36. Loh Z, Fitzsimmons RL, Reid RC, Ramnath D, Clouston A, Gupta PK, Irvine KM, Powell EE, Schroder K, Stow JL, et al. (2019). Inhibitors of class I histone deacetylases attenuate thioacetamide-induced liver fibrosis in mice by suppressing hepatic type 2 inflammation. Br. J. Pharmacol 176, 3775–3790. 10.1111/bph.14768. [PubMed: 31236923]

37. Mannaerts I, Nuytten NR, Rogiers V, Vanderkerken K, van Grunsven LA, and Geerts A (2010). Chronic administration of valproic acid inhibits activation of mouse hepatic stellate cells in vitro and in vivo. Hepatology 51, 603–614. 10.1002/hep.23334. [PubMed: 19957378]
38. Robey RB, and Hay N (2006). Mitochondrial hexokinases, novel mediators of the antiapoptotic effects of growth factors and Akt. Oncogene 25, 4683–4696. 10.1038/sj.onc.1209595. [PubMed: 16892082]
39. Wang F, Jia Y, Li M, Wang L, Shao J, Guo Q, Tan S, Ding H, Chen A, Zhang F, et al. (2019). Blockade of glycolysis-dependent contraction by oroxylin a via inhibition of lactate dehydrogenase-a in hepatic stellate cells. Cell Commun. Signal 17, 11. 10.1186/s12964-019-0324-8. [PubMed: 30744642]
40. Zheng D, Jiang Y, Qu C, Yuan H, Hu K, He L, Chen P, Li J, Tu M, Lin L, et al. (2020). Pyruvate kinase M2 tetramerization protects against hepatic stellate cell activation and liver fibrosis. Am. J. Pathol 190, 2267–2281. 10.1016/j.ajpath.2020.08.002. [PubMed: 32805235]
41. Pan RY, He L, Zhang J, Liu X, Liao Y, Gao J, Liao Y, Yan Y, Li Q, Zhou X, et al. (2022). Positive feedback regulation of microglial glucose metabolism by histone H4 lysine 12 lactylation in Alzheimer's disease. Cell Metab 34, 634–648.e6. 10.1016/j.cmet.2022.02.013. [PubMed: 35303422]
42. Moreno-Yruela C, Zhang D, Wei W, Bæk M, Liu W, Gao J, Danková D, Nielsen AL, Bolding JE, Yang L, et al. (2022). Class I histone deacetylases (HDAC1–3) are histone lysine delactylases. Sci. Adv 8, eabi6696. 10.1126/sciadv.abi6696. [PubMed: 35044827]
43. Barcena-Varela M, Colyn L, and Fernandez-Barrena MG (2019). Epigenetic mechanisms in hepatic stellate cell activation during liver fibrosis and carcinogenesis. Int. J. Mol. Sci 20, 2507. 10.3390/ijms20102507. [PubMed: 31117267]
44. Barcena-Varela M, Paish H, Alvarez L, Uriarte I, Latasa MU, Santamaria E, Recalde M, Garate M, Claveria A, Colyn L, et al. (2021). Epigenetic mechanisms and metabolic reprogramming in fibrogenesis: dual targeting of G9a and DNMT1 for the inhibition of liver fibrosis. Gut 70, 388–400. 10.1136/gutjnl-2019-320205. [PubMed: 32327527]
45. San José-Enériz E, Agirre X, Rabal O, Vilas-Zornoza A, Sanchez-Arias JA, Miranda E, Ugarte A, Roa S, Paiva B, Estella-Hermoso de Mendoza A, et al. (2017). Discovery of first-in-class reversible dual small molecule inhibitors against G9a and DNMTs in hematological malignancies. Nat. Commun 8, 15424. 10.1038/ncomms15424. [PubMed: 28548080]
46. Weiskirchen R, Weimer J, Meurer SK, Kron A, Seipel B, Vater I, Arnold N, Siebert R, Xu L, Friedman SL, et al. (2013). Genetic characteristics of the human hepatic stellate cell line LX-2. PLoS One 8, e75692. 10.1371/journal.pone.0075692. [PubMed: 24116068]
47. Kaya-Okur HS, Janssens DH, Henikoff JG, Ahmad K, and Henikoff S (2020). Efficient low-cost chromatin profiling with CUT&Tag. Nat. Protoc 15, 3264–3283. 10.1038/s41596-020-0373-x. [PubMed: 32913232]
48. Dobin A, Davis CA, Schlesinger F, Drenkow J, Zaleski C, Jha S, Batut P, Chaisson M, and Gingeras TR (2013). STAR: ultrafast universal RNA-seq aligner. Bioinformatics 29, 15–21. 10.1093/bioinformatics/bts635. [PubMed: 23104886]
49. Robinson MD, McCarthy DJ, and Smyth GK (2010). edgeR: a Bioconductor package for differential expression analysis of digital gene expression data. Bioinformatics 26, 139–140. 10.1093/bioinformatics/btp616. [PubMed: 19910308]
50. Bray NL, Pimentel H, Melsted P, and Pachter L (2016). Near-optimal probabilistic RNA-seq quantification. Nat. Biotechnol 34, 525–527. 10.1038/nbt.3519. [PubMed: 27043002]
51. Langmead B, and Salzberg SL (2012). Fast gapped-read alignment with Bowtie 2. Nat. Methods 9, 357–359. 10.1038/nmeth.1923. [PubMed: 22388286]
52. Li H, Handsaker B, Wysoker A, Fennell T, Ruan J, Homer N, Marth G, Abecasis G, and Durbin R; 1000 Genome Project Data Processing Subgroup (2009). The Sequence Alignment/Map format and SAMtools. Bioinformatics 25, 2078–2079. 10.1093/bioinformatics/btp352. [PubMed: 19505943]
53. Meers MP, Tenenbaum D, and Henikoff S (2019). Peak calling by Sparse Enrichment Analysis for CUT&RUN chromatin profiling. Epigenetics Chromatin 12, 42. 10.1186/s13072-019-0287-4. [PubMed: 31300027]

54. Yu G, Wang LG, and He QY (2015). ChIPseeker: an R/Bioconductor package for ChIP peak annotation, comparison and visualization. Bioinformatics 31, 2382–2383. 10.1093/bioinformatics/btv145. [PubMed: 25765347]

55. Ramírez F, Dündar F, Diehl S, Grüning BA, and Manke T (2014). deepTools: a flexible platform for exploring deep-sequencing data. Nucleic Acids Res 42. W187–W191. 10.1093/nar/gku365. [PubMed: 24799436]

56. Thorvaldsdóttir H, Robinson JT, and Mesirov JP (2013). Integrative Genomics Viewer (IGV): high-performance genomics data visualization and exploration. Brief. Bioinform 14, 178–192. 10.1093/bib/bbs017. [PubMed: 22517427]

57. Bankhead P, Loughrey MB, Fernández JA, Dombrowski Y, McArt DG, Dunne PD, McQuaid S, Gray RT, Murray LJ, Coleman HG, et al. (2017). QuPath: open source software for digital pathology image analysis. Sci. Rep 7, 16878. 10.1038/s41598-017-17204-5. [PubMed: 29203879]

58. Varghese F, Bukhari AB, Malhotra R, and De A (2014). IHC Profiler: an open source plugin for the quantitative evaluation and automated scoring of immunohistochemistry images of human tissue samples. PLoS One 9, e96801. 10.1371/journal.pone.0096801. [PubMed: 24802416]

59. Tag CG, Sauer-Lehnen S, Weiskirchen S, Borkham-Kamphorst E, Tolba RH, Tacke F, and Weiskirchen R (2015). Bile duct ligation in mice: induction of inflammatory liver injury and fibrosis by obstructive cholestasis. J. Vis. Exp 10.3791/52438.

60. Mederacke I, Dapito DH, Affò S, Uchinami H, and Schwabe RF (2015). High-yield and high-purity isolation of hepatic stellate cells from normal and fibrotic mouse livers. Nat. Protoc 10, 305–315. 10.1038/nprot.2015.017. [PubMed: 25612230]

61. Shechter D, Dormann HL, Allis CD, and Hake SB (2007). Extraction, purification and analysis of histones. Nat. Protoc 2, 1445–1457. 10.1038/nprot.2007.202. [PubMed: 17545981]

62. Buenrostro JD, Wu B, Litzenburger UM, Ruff D, Gonzales ML, Snyder MP, Chang HY, and Greenleaf WJ (2015). Single-cell chromatin accessibility reveals principles of regulatory variation. Nature 523, 486–490. 10.1038/nature14590. [PubMed: 26083756]

Highlights

- Histone lactylation is elevated by HK2 induction during HSC activation
- H3K18la is enriched at the promoter of HSC activation-induced genes
- HSC-specific or systemic deletion of HK2 ameliorates liver fibrosis
- Supplement of lactate overcomes HK2 deletion to promote liver fibrosis

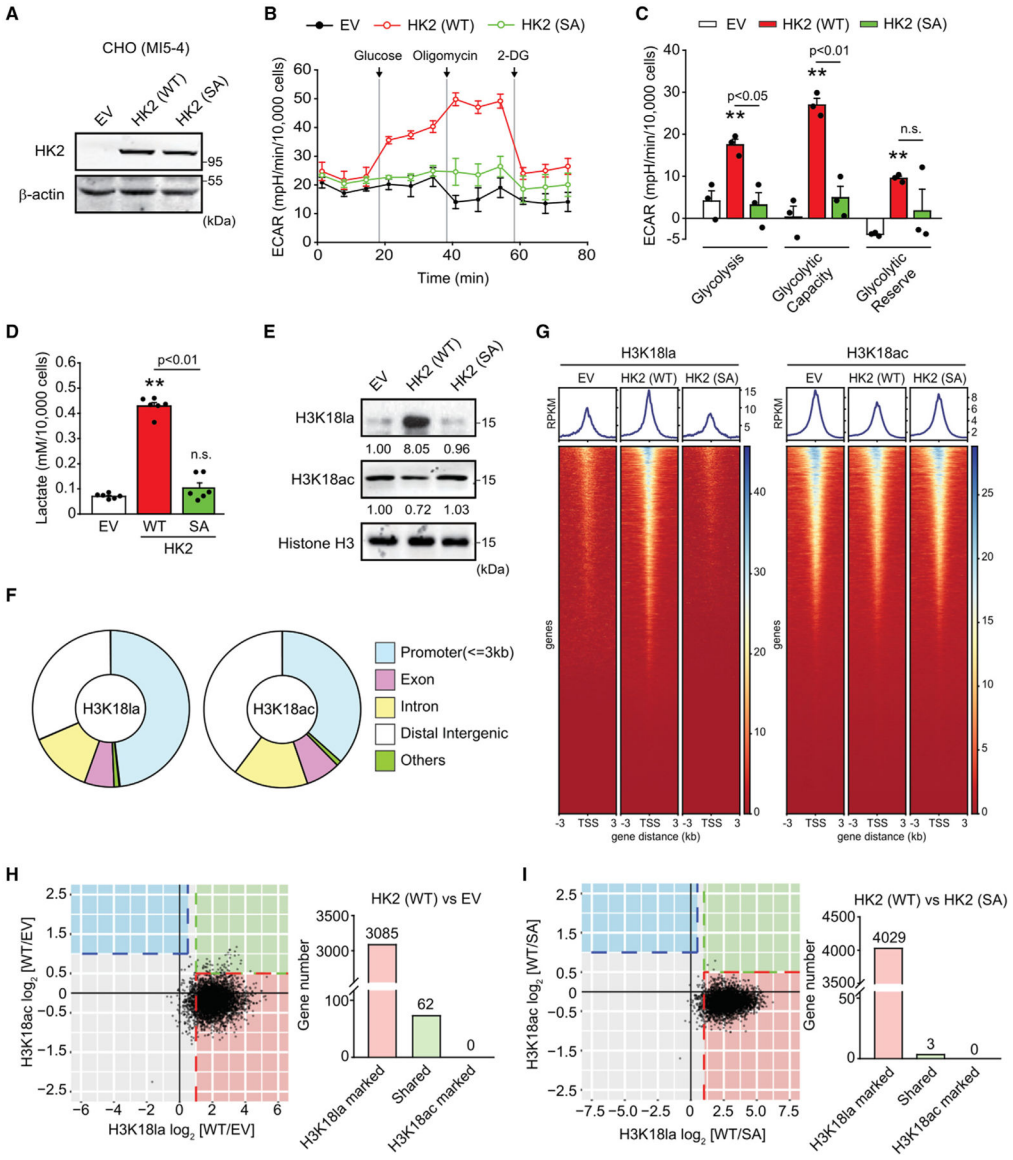

Figure 1. HK2 expression induces glycolysis, lactate production, and histone lactylation in MI5–4 CHO cells

(A) Immunoblot showing HK2 expression in CHO (MI5–4) cells expressing an empty vector (EV), wild-type (WT) HK2, or kinase-dead mutant (SA) HK2.

(B and C) Seahorse metabolic analysis (ECAR) of EV-, WT HK2- and SA HK2-expressing CHO (MI5–4) cells (n = 3).

(D) Measurement of lactate production in EV-, WT HK2-, and SA HK2-expressing CHO (MI5–4) cells (n = 6).

(E) Immunoblot showing H3K18la and H3K18ac in EV-, WT HK2-, and SA HK2-expressing CHO (MI5–4) cells.

(F) Pie chart showing the distribution of H3K18la and H3K18ac at annotated genomic regions in CHO (MI5–4) cells expressing WT HK2.

(G) Heatmap showing the genomic occupancy of H3K18la and H3K18ac ± 3 kb flanking TSSs in EV-, WT HK2-, and SA HK2-expressing CHO (MI5–4) cells. The genes shown in rows are sorted in descending order by signal strength.

(H) Scatterplot (left) and bar plot (right) showing genes with promoters marked by increases in only H3K18la (H3K18la $\log_2$[WT/EV] ≥ 1 and H3K18ac $\log_2$[WT/EV] < 0.5; H3K18la-marked candidate genes), increases in both H3K18la and H3K18ac (H3K18la $\log_2$[WT/EV] ≥ 1 and H3K18ac $\log_2$[WT/EV] ≥ 0.5; shared candidate genes), or increases in only H3K18ac (H3K18la $\log_2$[WT/EV] ≤ 0.5 and H3K18ac $\log_2$[WT/EV] ≥ 1; H3K18ac-marked candidate genes).

(I) Scatterplot (left) and bar plot (right) showing genes with promoters marked by increases in only H3K18la (H3K18la $\log_2$[WT/SA] ≥ 1 and H3K18ac $\log_2$[WT/SA] < 0.5; H3K18la-marked candidate genes), increases in both H3K18la and H3K18ac (H3K18la $\log_2$[WT/SA] ≥ 1 and H3K18ac $\log_2$[WT/SA] ≥ 0.5; shared candidate genes), or increases in only H3K18ac (H3K18la $\log_2$[WT/SA] ≤ 0.5 and H3K18ac $\log_2$[WT/SA] ≥ 1; H3K18ac-marked candidate genes).

The statistical significance of the differences was determined by one-way ANOVA with (C) SNK (Student-Newman-Keuls) post hoc analysis or (D) Tukey’s post hoc analysis (n.s., not significant; **p < 0.01 versus EV).

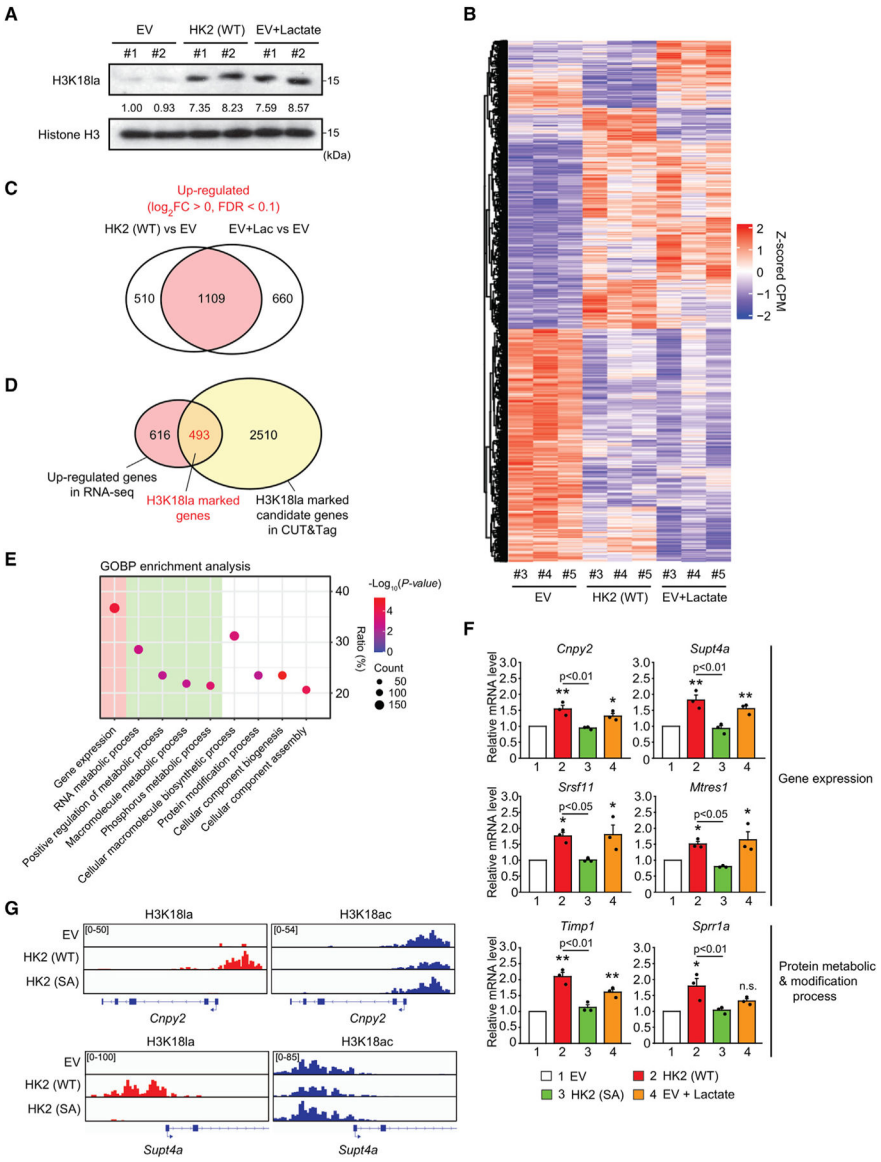

Figure 2. HK2/H3K18la-specific genes are involved in the regulation of gene expression and various metabolic processes in MI5–4 CHO cells

(A) Immunoblot showing H3K18la in CHO (MI5–4) cells expressing the empty vector (EV), wild-type (WT) HK2, or the EV with 10 mM lactate treatment for 24 h.

(B) Heatmap representing the differential gene expression in CHO (MI5–4) cells as in (A). The color bar represents the Z-transformed expression values.

In (A) and (B), cells were seeded in separate plates (#1–#5) simultaneously. Plates #1 and #2 were collected for immunoblotting. Plates #3, #4, and #5 were collected for RNA-seq.

(C) Venn diagram depicting the number of upregulated genes in WT HK2 cells versus EV cells and lactate-treated EV cells versus EV CHO (MI5–4) cells. The overlapping genes were designated as upregulated genes in RNA-seq in (D).

(D) Venn diagram depicting the number of H3K18la-marked genes in CHO (MI5–4) cells. The overlapping genes in (C) were designated as upregulated genes in RNA-seq. The

overlapping genes in Figure S1G were designated H3K18la-marked candidate genes in CUT&Tag. See also Table S1.

(E) GOBP enrichment analysis of H3K18la-marked genes defined as in (D). The x axis is the GOBP term, and the y axis is the gene ratio representing the proportion of enriched genes in the GOBP term to the number of genes in the input gene list. The size and color of the dot represent the number of genes associated with the GOBP term and the significance, respectively. The list of genes was analyzed in *mus musculus* background in DAVID database. See also Table S2.

(F) *Cnpy2*, *Supt4a*, *Srsf11*, *Mtres1*, *Timp1*, and *Sprr1a* mRNA expression in EV-, WT HK2-, SA HK2-, and EV-expressing cells treated with 10 mM lactate for 24 h (n = 3).

(G) Normalized read densities for H3K18la and H3K18ac at the *Cnpy2* and *Supt4a* genes.

The statistical significance of the differences between groups was determined by (F) one-way ANOVA with SNK post hoc analysis (n.s., not significant; *$p < 0.05$, **$p < 0.01$ versus EV).

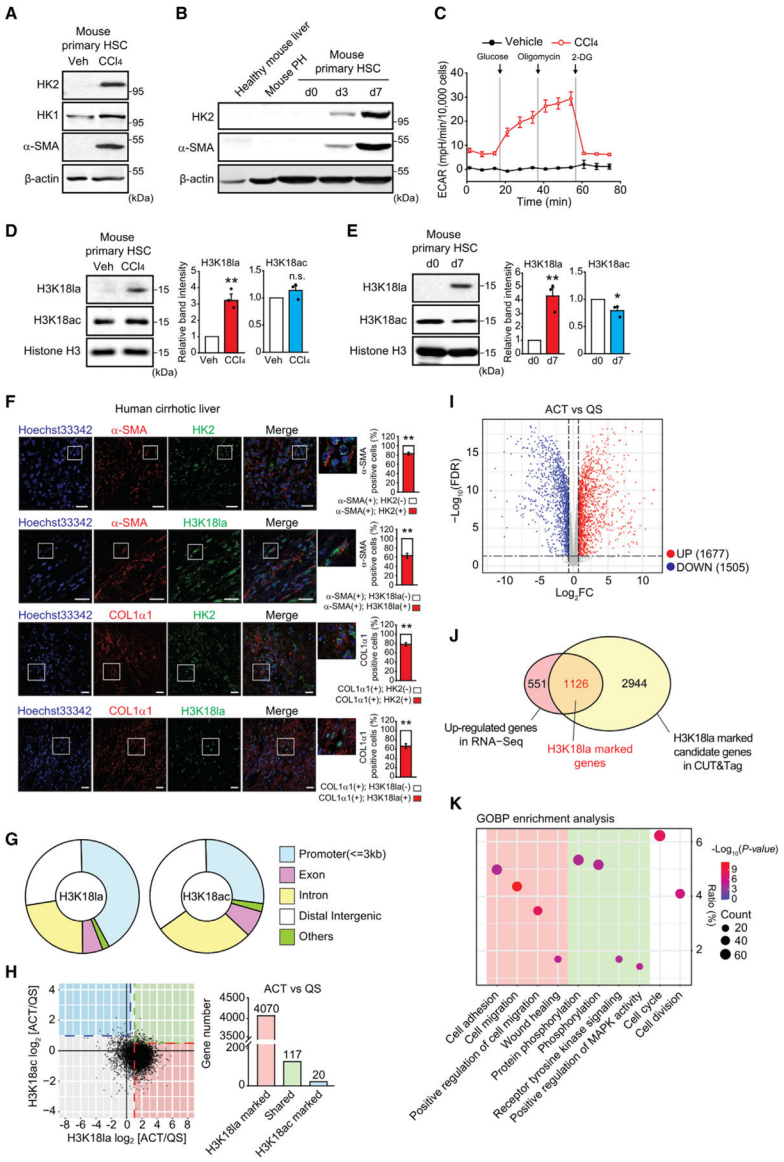

Figure 3. HK2/H3K18la is induced and regulates gene expression during HSC activation

(A) Immunoblot showing HK2, HK1, and α-SMA levels in mouse primary HSCs freshly isolated from the livers of mice treated with vehicle or CCl_4 (0.5 mL/kg body weight, i.p.) twice a week for 3 weeks.

(B) Immunoblot showing HK2 and α-SMA levels in mouse primary HSCs cultured for 3–7 days (mouse PH, mouse primary hepatocyte).

(C) Seahorse metabolic analysis (ECAR) of mouse primary HSCs isolated from livers and similarly treated as in (A) (n = 3).

(D) Immunoblot (left) and relative band intensity (right) of H3K18la and H3K18ac in mouse primary HSCs isolated from the livers of mice treated as in (A) (n = 3).

(E) Immunoblot (left) and relative band intensity (right) of H3K18la and H3K18ac in mouse primary HSCs isolated from mouse livers and cultured for 7 days (n = 3).

(F) Representative double immunofluorescence staining images of α-SMA, COL1α1, HK2, and H3K18la in human livers from patients with cirrhosis (scale bars, 20 μm). The boxed regions are shown at higher magnification.
(G) Pie chart showing the distribution of H3K18la and H3K18ac at annotated genomic regions in activated mouse primary HSCs cultured for 6 days.
(H) Scatterplot (left) and bar plot (right) showing genes with promoters marked by increases in only H3K18la (H3K18la $\log_2$[ACT/QS] ≥ 1 and H3K18ac $\log_2$[ACT/QS] < 0.5; H3K18la-marked candidate genes), increases in both H3K18la and H3K18ac (H3K18la $\log_2$[ACT/QS] ≥ 1 and H3K18ac $\log_2$[ACT/QS] ≥ 0.5; shared candidate genes), or increases in only H3K18ac (H3K18la $\log_2$[ACT/QS] ≤ 0.5 and H3K18ac $\log_2$[ACT/QS] ≥ 1; H3K18ac-marked candidate genes).
(I) Volcano plot depicting the differential gene expression between activated and quiescent mouse primary HSCs. Significantly upregulated genes are shown in red (false discovery rate [FDR] < 0.05 and $\log_2$[fold change] > 0.5), and significantly downregulated genes are shown in blue (FDR < 0.05 and $\log_2$[fold change] < 0.5). All other genes are shown in gray. In (H) and (I), mouse primary HSCs freshly isolated from mouse liver were considered quiescent HSCs, and the cells cultured for 6 days were considered activated HSCs (denoted QS and ACT, respectively).
(J) Venn diagram depicting the number of H3K18la-marked genes in activated HSCs. The significantly upregulated genes in (I) were designated as upregulated genes in RNA-seq. The H3K18la-marked candidate genes in (H) were designated H3K18la-marked candidate genes in CUT&Tag. See also Table S3.
(K) GOBP enrichment analysis of H3K18la-marked genes defined as in (J). The x axis is the GOBP term, and the y axis is the gene ratio representing the proportion of enriched genes in the GOBP term to the number of genes in the input gene list. The size and color of the dot represent the number of genes associated with the GOBP term and the significance, respectively. See also Table S4.
The statistical significance of the differences between groups was determined by (D–F) unpaired two-tailed Student's t test (n.s., not significant; *p < 0.05, **p < 0.01 versus vehicle or day 0; **p < 0.01 versus α-SMA(+)HK2(−) or α-SMA(+)H3K18la(−); COL1α1(+)HK2(−) or COL1α1(+);H3K18la(−)).

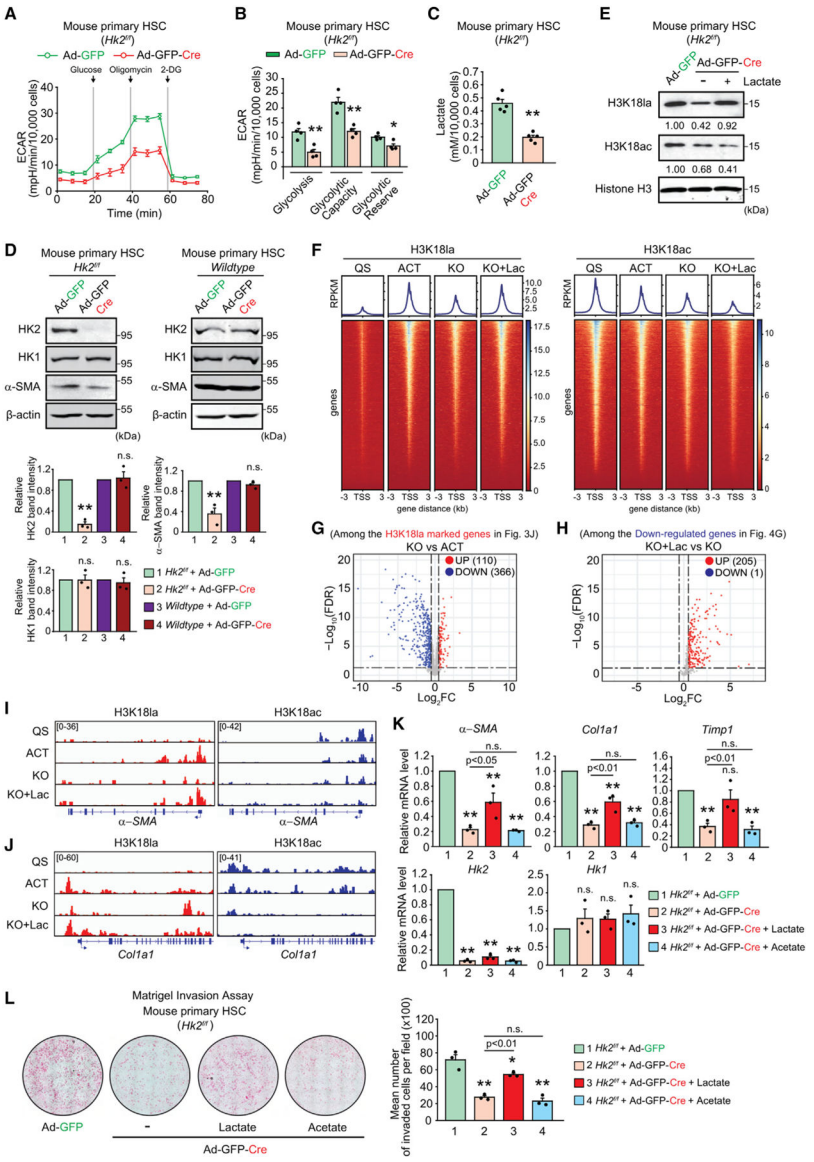

Figure 4. Genetic deletion of *Hk2* inhibits HSC activation by reducing H3K18la, which is rescued by exogenous lactate but not acetate treatment

(A and B) Seahorse metabolic analysis (ECAR) of *Hk2*-deleted mouse primary HSCs (n = 4).

(C) Measurement of lactate production in *Hk2*-deleted mouse primary HSCs (n = 5).

(D) Immunoblot (upper) and relative band intensity (bottom) of HK2, HK1, and α-SMA in *Hk2*-deleted or control wild-type mouse primary HSCs (n = 3).

(E) Immunoblot showing H3K18la and H3K18ac in *Hk2*-deleted mouse primary HSCs similarly treated as in (D) except for 10 mM lactate treatment for 24 h.

In (A)–(E), mouse primary HSCs were freshly isolated from *Hk2*$^{f/f}$ mouse livers and transduced with adenoviruses encoding GFP (Ad-GFP) or GFP-Cre (Ad-GFP-Cre) to generate *Hk2*-deleted HSCs.

(F) Heatmap showing the genomic occupancy of H3K18la and H3K18ac ± 3 kb flanking TSSs in quiescent, activated, *Hk2*-deleted, and 10 mM lactate-treated *Hk2*-deleted mouse primary HSCs. The genes shown in rows are sorted in descending order by signal strength.
(G) Volcano plot depicting the differential gene expression between *Hk2*-deleted and control activated mouse primary HSCs. Only the H3K18la-marked genes defined in Figure 3J were analyzed.
(H) Volcano plot depicting the differential gene expression between *Hk2*-deleted and lactate-treated *Hk2*-deleted mouse primary HSCs. Only the significantly downregulated genes defined in (G) were analyzed. See also Table S5.
In (G) and (H), significantly upregulated genes are shown in red (FDR < 0.05 and $\log_2$[fold change] > 0.5), and significantly downregulated genes are shown in blue (FDR < 0.05 and $\log_2$[fold change] < 0.5). All other genes are shown in gray.
(I and J) Normalized read densities for H3K18la and H3K18ac at the *α-SMA* and *Col1a1* genes.
In (F)–(J), mouse primary HSCs freshly isolated from mouse livers were considered quiescent HSCs, and the cells cultured for 6 days were considered activated HSCs (denoted QS and ACT, respectively). Mouse primary HSCs from *Hk2*$^{f/f}$ mouse livers transduced with adenovirus encoding GFP-Cre (Ad-GFP-Cre) and cultured for 6 days were considered *Hk2*-knockout HSCs (denoted KO). *Hk2*-deleted HSCs treated with 10 mM lactate for 24 h are denoted KO + Lac.
(K) *α-SMA*, *Col1a1*, *Timp1*, *Hk2*, and *Hk1* mRNA expression in *Hk2*-deleted mouse primary HSCs similarly treated as in (E) except for 10 mM acetate treatment for 24 h (n = 3).
(L) Microscopic images (left) of the Matrigel invasion capacity of mouse primary HSCs similarly treated as in (K). Representative images are shown. The bar plot (right) shows the mean number of invaded cells per field (×100, n = 3–5 for each group).
In (K) and (L), mouse primary HSCs from *Hk2*$^{f/f}$ mouse livers were transduced with adenoviruses encoding GFP (Ad-GFP) or GFP-Cre (Ad-GFP-Cre) to generate *Hk2*-deleted HSCs.
The statistical significance of the differences between groups was determined by (B–D) unpaired two-tailed Student's t test or (K and L) one-way ANOVA with Tukey's post hoc analysis (n.s., not significant; *p < 0.05, **p < 0.01 versus Ad-GFP).

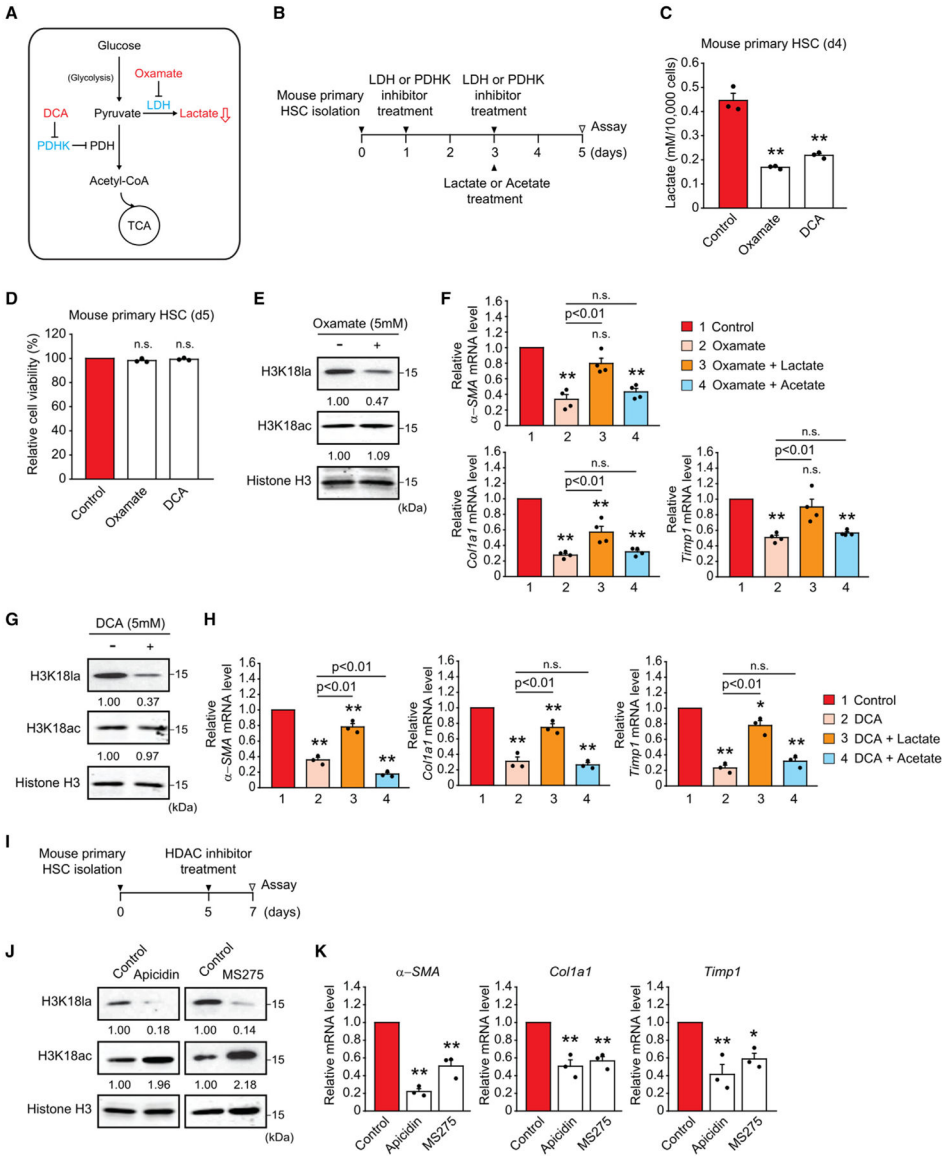

Figure 5. Decreased H3K18la by inhibiting lactate production or class I HDAC inhibitor treatment inactivates HSCs

(A) Schematic depicting the inhibition of lactate production by oxamate and DCA treatments (LDH, lactate dehydrogenase; PDH, pyruvate dehydrogenase; PDHK, pyruvate dehydrogenase kinase; TCA, tricarboxylic acid cycle; DCA, dichloroacetate).

(B) Schematic of the experimental design using an LDH or PDHK inhibitor in the absence or presence of lactate or acetate treatment in mouse primary HSCs.

(C) Measurement of lactate production in activated mouse primary HSCs treated with 5 mM oxamate and 5 mM DCA (n = 3).

(D) Relative cell viability of activated mouse primary HSCs treated with 5 mM oxamate and 5 mM DCA (n = 3).

(E) Immunoblot showing H3K18la and H3K18ac in activated mouse primary HSCs treated with 5 mM oxamate.

(F) *α-SMA*, *Col1a1*, and *Timp1* mRNA expression in activated mouse primary HSCs similarly treated as in (E) except for 10 mM lactate or acetate treatment for 48 h (n = 4).

(G) Immunoblot showing H3K18la and H3K18ac in activated mouse primary HSCs following 5 mM DCA treatment.

(H) *α-SMA*, *Col1a1*, and *Timp1* mRNA expression in activated mouse primary HSCs similarly treated as in (F) except for 5 mM DCA treatment (n = 3).

(I) Schematic illustrating the experimental design using class I HDAC inhibitor treatment in activated mouse primary HSCs.

(J) Immunoblot showing H3K18la and H3K18ac in activated mouse primary HSCs treated with 1 mM apicidin and MS275.

(K) *α-SMA*, *Col1a1*, and *Timp1* mRNA expression in activated mouse primary HSCs treated with class I HDAC inhibitors as in (J) (n = 3).

The statistical significance of the differences between groups was determined by (C and D) unpaired two-tailed Student's t test or (F, H, and K) one-way ANOVA with Tukey's post hoc analysis (n.s., not significant; *$p < 0.05$, **$p < 0.01$ versus control).

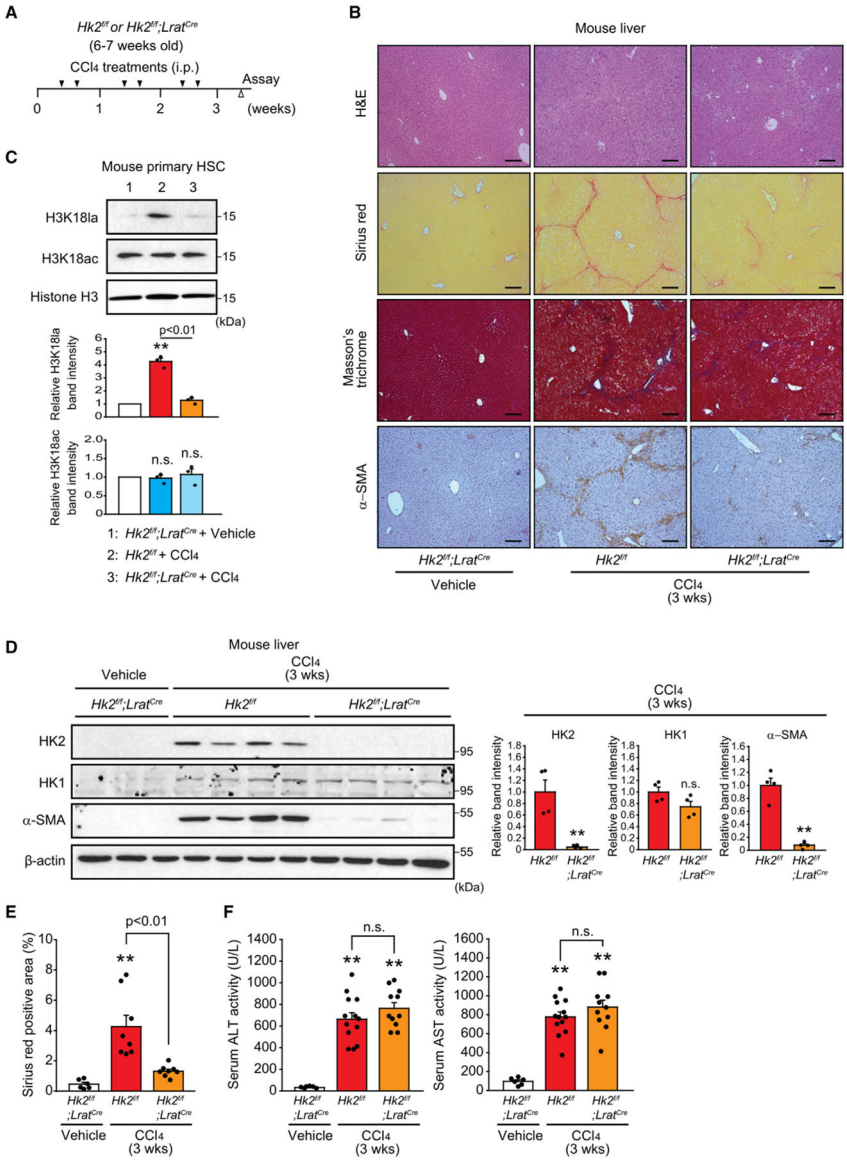

Figure 6. Specific deletion of *Hk2* in HSCs ameliorates CCl_4-induced liver fibrosis

(A) Schematic illustrating the experimental design of liver fibrosis induction after *in vivo* deletion of *Hk2* specifically in HSCs. $Hk2^{f/f}$ or $Hk2^{f/f};Lrat^{Cre}$ mice were injected with vehicle or CCl_4 (0.5 mL/kg body weight, i.p.) twice a week for 3 weeks (n = 6–13 for each group).

(B) Representative images of H&E, Sirius red, Masson's trichrome staining, and IHC staining images of α-SMA in $Hk2^{f/f}$ or $Hk2^{f/f};Lrat^{Cre}$ liver sections of mice treated as described in (A) (scale bars, 100 μm).

(C) Immunoblot (upper) and relative band intensity (bottom) of H3K18la and H3K18ac in mouse primary HSCs isolated from mouse livers similarly treated as in (A) (n = 3).

(D) Immunoblot (left) and relative band intensity (right) of HK2, HK1, and α-SMA in the livers of $Hk2^{f/f}$ or $Hk2^{f/f};Lrat^{Cre}$ mice treated as described in (A).

(E) Quantification of the Sirius red-positive area (collagen) in the livers of $Hk2^{f/f}$ or $Hk2^{f/f};Lrat^{Cre}$ mice treated as described in (A).

(F) Serum alanine transaminase (ALT) and aspartate transaminase (AST) activities in $Hk2^{f/f}$ or $Hk2^{f/f};Lrat^{Cre}$ mice treated as described in (A).

The statistical significance of the differences between groups was determined by (D) unpaired two-tailed Student's t test (n.s., not significant; **$p < 0.01$ versus $Hk2^{f/f}$ with CCl_4) or (C, E, and F) one-way ANOVA with Tukey's post hoc analysis (n.s., not significant; **$p < 0.01$ versus vehicle).

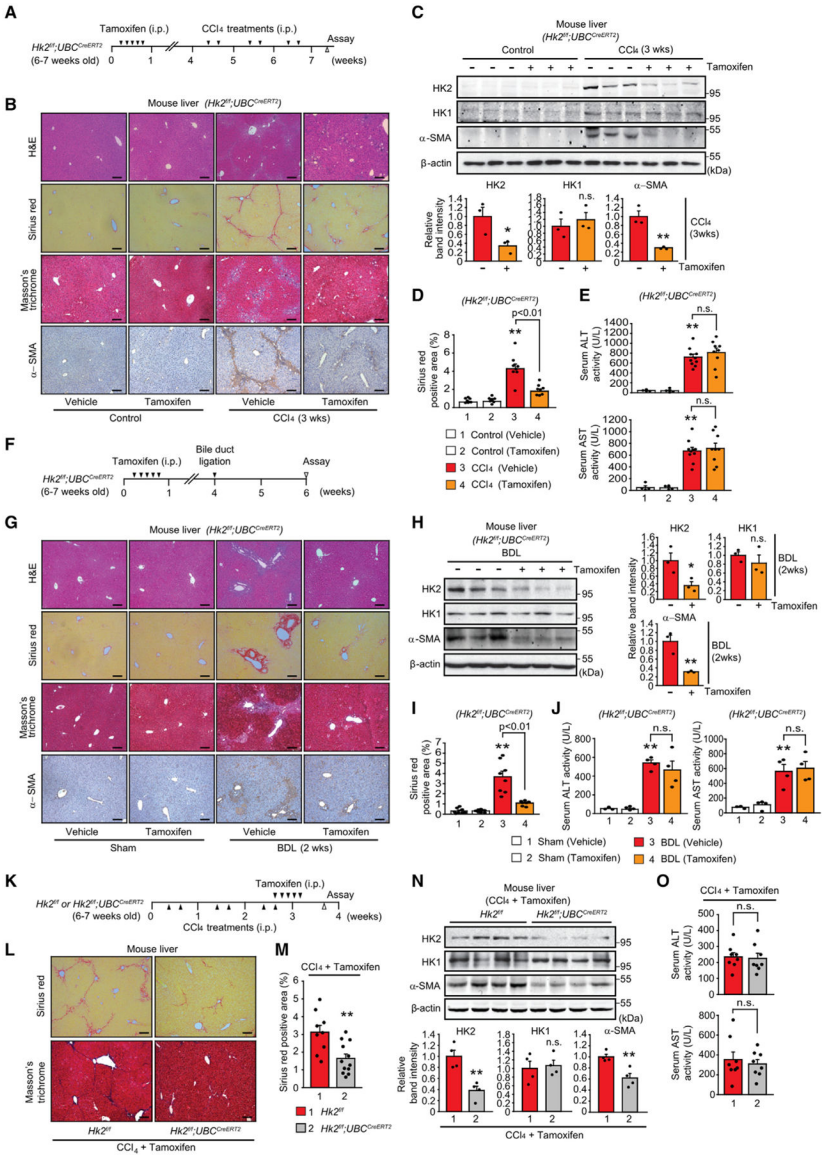

Figure 7. Inhibition of CCl_4-induced and BDL-induced liver fibrosis by systemic deletion of *Hk2 in vivo*

(A) Schematic illustrating the experimental design of liver fibrosis induction by CCl_4 in *Hk2*$^{f/f}$;*UBC*^{CreERT2} mice treated or untreated with tamoxifen (n = 4–9 for each group).

(B) Representative images of H&E, Sirius red, Masson's trichrome staining, and IHC staining images of α-SMA in liver sections of mice treated as described in (A) (scale bar, 100 μm).

(C) Immunoblot (upper) and relative band intensity (bottom) of HK2, HK1, and α-SMA in the livers of the mice described in (A).

(D) Quantification of the Sirius red-positive area (collagen) in the livers of mice treated as described in (A).

(E) Serum alanine transaminase (ALT) and aspartate transaminase (AST) activities in the mice described in (A).

(F) Schematic illustrating the experimental design of liver fibrosis induction by BDL in *Hk2*$^{f/f}$;*UBC*^{CreERT2} mice treated or untreated with tamoxifen (n = 3–5 for each group).
(G) Representative images of H&E, Sirius red, Masson's trichrome staining, and IHC staining images of α-SMA in liver sections of the mice described in (F) (scale bar, 100 μm).
(H) Immunoblot (left) and relative band intensity (right) of HK2, HK1, and α-SMA in the livers of the mice described in (F).
(I) Quantification of the Sirius red-positive area (collagen) in the livers of mice treated as described in (F).
(J) Serum alanine transaminase (ALT) and aspartate transaminase (AST) activities in mice described as in (F).
(K) Schematic illustrating the experimental design of *Hk2* deletion after liver fibrosis induction by CCl_4 in *Hk2*$^{f/f}$ or *Hk2*$^{f/f}$;*UBC*^{CreERT2} mice (n = 8–10 for each group).
(L) Representative images of Sirius red and Masson's trichrome staining in liver sections of mice treated as described in (K) (scale bar, 100 μm).
(M) Quantification of the Sirius red-positive area (collagen) in the livers of mice treated as described in (K).
(N) Immunoblot (upper) and relative band intensity (bottom) of HK2, HK1, and α-SMA in the livers of the mice treated as described in (K).
(O) Serum alanine transaminase (ALT) and aspartate transaminase (AST) activities in mice as described in (K).
The statistical significance of the differences between groups was determined by (C, H, and M–O) unpaired two-tailed Student's t test (n.s., not significant; *$p < 0.05$, **$p < 0.01$ versus *Hk2*$^{f/f}$; *UBC*^{CreERT2} in CCl_4 or in BDL or *Hk2*$^{f/f}$ with CCl_4 + tamoxifen) or (D, E, I, and J) one-way ANOVA with Tukey's post hoc analysis (n.s., not significant; **$p < 0.01$ versus vehicle or sham control).

KEY RESOURCES TABLE

REAGENT or RESOURCE	SOURCE	IDENTIFIER
Hexokinase 2 (C64G5) rabbit mAb	Cell Signaling Technology	Cat#2867; RRID:AB_2232946
Hexokinase 2 polyclonal antibody	Proteintech	Cat#22029–1-AP; RRID:AB_11182717
HK1 monoclonal antibody (7A7)	Invitrogen	Cat#MA5–15675; RRID:AB_10983588
Alpha smooth muscle actin antibody [1A4]	Abcam	Cat#ab7817; RRID:AB_262054
COL1A1 mouse mAb	Cell Signaling Technology	Cat#66948; RRID:AB_2920541
Monoclonal anti-β-actin antibody	Sigma	Cat#A5441; RRID:AB_476744
β-actin (13E5) rabbit mAb	Cell Signaling Technology	Cat#4970; RRID:AB_2223172
GCK antibody (H-88)	Santa Cruz Biotechnology	Cat#sc-7908; RRID:AB_2107620
Anti-L-lactyllysine rabbit pAb	PTM Biolabs	Cat#PTM-1401; RRID:AB_2868521
Lactyl-histone H3 (Lys18) rabbit pAb	PTM Biolabs	Cat#PTM-1406
Lactyl-histone H3 (Lys18) rabbit mAb	PTM Biolabs	Cat#PTM-1406RM; RRID:AB_2909438
Lactyl-histone H3 (Lys18) rabbit mAb	PTM Biolabs	Cat#PTM-1427RM
Lactyl-histone H3 (Lys9) rabbit mAb	PTM Biolabs	Cat#PTM1419RM
Lactyl-histone H3 (Lys14) rabbit pAb	PTM Biolabs	Cat#PTM-1414
Lactyl-histone H4 (Lys8) rabbit pAb	PTM Biolabs	Cat#PTM-1415
Lactyl-histone H4 (Lys12) rabbit mAb	PTM Biolabs	Cat#PTM-1411RM
Acetylated-Lysine antibody	Cell Signaling Technology	Cat#9441; RRID:AB_331805
Anti-histone H3 (acetyl K18) antibody	Abcam	Cat#ab1191; RRID:AB_298692
Histone H3 antibody	Cell Signaling Technology	Cat#9715; RRID:AB_331563
Histone H3 (96C10) mouse mAb	Cell Signaling Technology	Cat#3638; RRID:AB_1642229
Phospho-pyruvate dehydrogenase a1 (Ser293) Antibody	Cell Signaling Technology	Cat#31866; RRID:AB_2799014
Anti-PDHA1 antibody [8D10E6]	Abcam	Cat#ab110334; RRID:AB_10866116
GAPDH (D16H11) XP rabbit mAb	Cell Signaling Technology	Cat#5174; RRID:AB_10622025
Goat anti-rabbit IgG (H+L) cross-adsorbed secondary antibody, alexa fluor 488	Invitrogen	Cat#A-11008; RRID:AB_143165
Goat anti-mouse IgG (H+L) cross-adsorbed secondary antibody, alexa fluor 594	Invitrogen	Cat#A-11005; RRID:AB_2534073
Monoclonal Mouse anti-Bromodeoxyuridine Clone Bu20a	Dako	Cat#M0744; RRID:AB_10013660
Rabbit (DA1E) mAb IgG XP Isotype Control	Cell Signaling Technology	Cat#3900; RRID:AB_1550038
Rabbit IgG negative control antibody	EpiCypher	Cat#13–0042; RRID:AB_2923178
IRDye 800CW goat anti rabbit IgG secondary antibody	LI-COR	Cat#926–32211; RRID:AB_621843
IRDye 680RD goat anti mouse IgG secondary antibody	LI-COR	Cat#926–68070; RRID:AB_10956588
Anti-rabbit secondary antibody	EpiCypher	Cat#13–0047
Bacterial and virus strains		

REAGENT or RESOURCE	SOURCE	IDENTIFIER
Ad5CMVeGFP	UI Viral Vector Core	Cat#Iowa-4
Ad5CMVCre-eGFP	UI Viral Vector Core	Cat#Iowa-1174
Biological samples		
Paraffin-embedded blocks of liver from patients with liver cirrhosis	https://tissuearray.com/	Cat#LV1602
Chemicals, peptides, and recombinant proteins		
Recombinant TGFβ1	Sigma-Aldrich	Cat#H8541
Carbon tetrachloride	Sigma-Aldrich	Cat#289116
Tamoxifen	Sigma-Aldrich	Cat#T5648
Pronase	Sigma-Aldrich	Cat#P5147
Collagenase, Type I	Worthington	Cat#LS004194
Deoxyribonuclease I	Worthington	Cat#LS002139
Nycodenz	Accurate Chemical and Scientific Corporation	Cat#AN1002424
MEM-α	US Biological Life Science	Cat#M3852–02
Sodium lactate	Sigma-Aldrich	L7022
Sodium acetate	Sigma-Aldrich	Cat#S5636
Sodium oxamate	Alfa Aesar	Cat#A16532
Sodium dichloroacetate	Sigma-Aldrich	Cat#347794
Apicidin	ApexBio	Cat#A8176
MS275 (Entionstat)	ApexBio	Cat#A8171
TRIzol	Invitrogen	Cat#15596–018
iScript cDNA Synthesis Kit	Bio-Rad	Cat#1708890
iQ SYBR Green Supermix	Bio-Rad	Cat#1708880
Direct-zol RNA MicroPrep Kit	Zymo Research	Cat#R2060
Concanavalin A-coated magnetic beads	EpiCypher	Cat#21–1401
CUTANA pAG-Tn5 for CUT&Tag	EpiCypher	Cat#15–1017
NEBNext High-Fidelity 2x PCR Master mix	New England Biolabs	Cat#M0541
AMPure XP beads	Beckman Coulter	Cat#A63880
BioCoat Matrigel Invasion Chamber	Corning	Cat#354480
On-Target plus Non-targeting siRNA#1	Dharmacon	Cat#D-001810–01-05
On-Target plus Mouse Ldha siRNA-SMART pool	Dharmacon	Cat#L-043884–00-0005
Lipofectamine 2000 Transfection Reagent	Invitrogen	Cat#11668019
Critical commercial assays		
EnzyChrom ALT Assay Kit	BioAssay Systems	Cat#EALT-100
EnzyChrom AST Assay Kit	BioAssay Systems	Cat#EASTR-100
Picoprobe L-Lactate Assay Kit	Abcam	Cat#ab169557
Acetyl-Coenzyme A Assay Kit	Sigma-Aldrich	Cat#MAK039
Pierce Rapid Gold BCA Protein Assay Kit	Thermo Scientific	Cat#A53225
Agilent Seahorse XF Glycolysis Stress Test Kit	Agilent Technologies	Cat#103020–100

REAGENT or RESOURCE	SOURCE	IDENTIFIER
Agilent Seahorse XF Cell Mito Stress Test Kit	Agilent Technologies	Cat#103015–100
Deposited data		
Raw sequencing data	This paper	GEO: GSE229156
Source Data (Data S1)	This paper	N/A
Experimental models: Cell lines		
Hamster: CHO (MI5–4) cells	Blaha et al.[24]	N/A
Human: Lx-2 cells	Provided by Dr. Scott L. Friedman (Icahn School of Medicine at Mount Sinai, NY)	N/A
Experimental models: Organisms/strains		
Mouse: *Hk2*$^{f/f}$;*UBC*^{CreERT2}	Patra et al.[6]	N/A
Mouse: *Lrat-Cre*	Provided by Dr. Robert F. Schwabe (Columbia University, NY)	N/A
Oligonucleotides		
Primers for qRT-PCR, see Table S7	This paper	N/A
Human *α-SMA* ChIP-qPCR forward primer: 5'-TTACCCTAGCTCAGTGTCTCTGG-3'	This paper	N/A
Human *α-SMA* ChIP-qPCR reverse primer: 5'-GGACCTCAGCACAAAACTCTCTA-3'	This paper	N/A
Recombinant DNA		
pLenti6-D-TOPO-Blast (Empty vector)	Invitrogen	Cat#K495510
pLenti6-Blast-WT HK2	Blaha et al.[24]	N/A
pLenti6-Blast-SA HK2	Blaha et al.[24]	N/A
pCW-Puro-WT HK2	This paper	N/A
Software and algorithms		
Agilent TapeStation Analysis	Agilent Technologies	N/A
STAR	Dobin et al.[48]	N/A
edgeR	Robinson et al.[49]	N/A
Kallisto	Bray et al.[50]	N/A
Bowtie2	Langmead and Salzberg[51]	N/A
Samtools	Li et al.[52]	N/A
SEACR	Meers et al.[53]	N/A
ChIPseeker	Yu et al.[54]	N/A
DeepTools	Ramirez et al.[55]	N/A
IGV	Thorvaldsdottir et al.[56]	N/A
QuPath	Bankhead et al.[57]	N/A
IHC Profiler	Varghese et al.[58]	N/A

REAGENT or RESOURCE	SOURCE	IDENTIFIER
Seahorse Wave Desktop	Agilent Technologies	N/A
SigmaPlot	Systat Software Incorporatoin	N/A